Surveys in Geophysics (2023) 44:877–923
https://doi.org/10.1007/s10712-022-09761-w

Characterization of Pore Electrical Conductivity in Porous Media by Weakly Conductive and Nonconductive Pores

Linqi Zhu[1,2] · Shiguo Wu[1,2] · Chaomo Zhang[3] · Siddharth Misra[4,5] · Xueqing Zhou[1,2] · Jianchao Cai[6]

Received: 24 November 2021 / Accepted: 14 December 2022 / Published online: 17 March 2023

Abstract

The formation factor, which reflects the electrical conductivity of porous sediments and rocks, is widely used in a range of research fields. Consequently, given the discovery of numerous porous reservoir rocks and sediments exhibiting complex conductivity characteristics, methods to quantitatively predict the formation factor have been actively pursued by many scholars. Nevertheless, the agreement between the theoretically calculated and measured formation factors remains unsatisfactory, partially because the distribution characteristics of the entire pore space affect the final formation factor. In this study, a new method for characterizing the formation factor is proposed that considers the impacts of different complex pore structures on the conductivity of pores at different positions in the pore space. With this method, the electrical transmission through a rock can be accurately and quantitatively estimated based on the conductivity and shape of pores, the tortuous conductivity, and the classification of the pore space into conductive, weakly conductive, and nonconductive pores. By evaluating 24 datasets encompassing 7 types of rocks and sediments, including marine hydrate-bearing sediments and shale, the proposed model achieves remarkable agreement with the experimental data. These excellent confirmation results are attributed to the ubiquitous presence of weakly conductive and nonconductive pores in almost all rocks and sediments. Through further research based on this paper, an increasing number of adaptation models and a comprehensive set of evaluation methods can be developed.

Keywords Formation factor · Truncated cone pore · Weakly conductive pores · Nonconductive pores · Porous media

Abbreviations

CWNM	Conductive pores + weakly conductive pores + nonconductive pores model
TPM	Trapezoidal model
CCM	Capillary channel model

✉ Shiguo Wu
swu@idsse.ac.cn

✉ Jianchao Cai
caijc@cup.edu.cn

Extended author information available on the last page of the article

EREM	Equivalent rock element model
PTM	Pore throat model
MRE	Mean relative error
CO_2	Carbon dioxide
H_2	Hydrogen

List of symbols

a	Tortuosity coefficient
$\overline{r_m}$	Average values along the radius
$r_{\max}$	Maximum radius
$r_{\max i}$	Type i-th maximum radius
$r_{\min}$	Minimum radius
$r_{\min j}$	j-th minimum radius
$r_{\min i}$	Type-i minimum radius
$\overline{r_{\min}}$	Average minimum values along the radius
r_{mi}	Radius value of pores with a pore scaling factor of c_{2i}
C	Pore structure efficiency
C_{d1}	Horizontal pore throat radius ratio
C_{d2}	Vertical pore throat radius ratio
c_1	Ratio of S to S_2
c_2	Pore scaling factor
c_{2i}	Pore scaling factor of type-i conductive pores
c_{2j}	Pore scaling factor of j-th conductive pores
c_3	Ratio of the cross-sectional area of weakly conductive pores to the sum of the cross-sectional areas of weakly conductive pores and nonconductive pores
E_o	Geometrical factor
e	Ratio of L_2 to L_1
e_{ps}	Volume ratio of conductive pores to weakly conductive pores
F	Formation factor
F_i	Number of corresponding truncated cone pores with circular cross sections whose radii are denoted $r_{\min i}$
F_j	Number of corresponding truncated cone pores with circular cross sections whose radii are denoted $r_{\min j}$
F_m	Formation factors measured experimentally or numerically
F_p	Formation factor evaluated using the equation
f_1	Proportion of total conductive pores
L	Length of the rock, dimensionless
L_g	Length of the truncated cone pore
L_w	Length of the pores in the rock
L_1	Length of the conductive pores
L_2	Length of weakly conductive pores or nonconductive pores
L_3	Length of nonconductive pores
m	Cementation factor, dimensionless
N	Number of conductive pores
P	Ratio between the radius of the minimum and average circular pore cross-sectional area
P_f	Pore along the electrical potential gradient

P_i	Ratio of the radius at the minimum cross-sectional area of the pores with pore scaling factor c_{2i} to the average radius
P_p	Pore perpendicular electrical potential gradient
P_p	Trapezoidal factor
Q	Ratio of conductive pores to total pores
R_{c1}	Throat radii in the horizontal direction
R_{c2}	Throat radii in the vertical direction
Rs	Half of the side length of a large pore
R_w	Brine resistivity (Ω m)
R_o	Resistivity of rocks saturated with brine (Ω m)
R_x	Ratio of the throat radius to the pore radius
r_b	Pore body radius
r_g	Resistance of a single truncated cone pore
r_{ma}	Resistance of the rock skeleton
r_c	Throat radius
r_o	Resistance of the rock
r_s	Pore radius
r_t	Pore throat radius
r_w	Resistance of the formation water
r_{1j}	Resistance of the j-th conductive pores
r_2	Resistance of the weakly conductive pore
$r(l)$	Corresponding radius value at length l of the pore
S	Cross-sectional area of the rock
S_b	Cross-sectional area of the capillary bundle pores in the rock
S_1	Cross-sectional area of the conductive pores
S_2	Cross-sectional area of the weakly conductive pores
S_3	Cross-sectional area of the nonconductive pores
$\overline{S}$	Average rock cross-sectional area
α	Pore shape factor
φ	Porosity, dimensionless
φ_c	Critical porosity
φ_p	Conductive porosity
φ_h	Weakly conductive porosity
φ_u	Nonconductive porosity
φ_{wne}	Ineffective conductive porosity
φ_x	Crossover porosity
σ_s	Surface conductivity (S/m)
σ_w	Brine conductivity (S/m)
σ_o	Conductivity of rocks saturated with brine (S/m)
τ_e	Electrical tortuosity of the pore space
λ_w	Percolation rate
γ_1	Ineffective conductive pore percolation coefficient
γ_2	Pore percolation coefficient
z	Ratio of L_3 to L_2

Article Highlights

- In the case of saturated brine, when rocks and sediments conduct electricity, the entire pore space will be divided into non-conductive pores, weakly conductive pores and conductive pores
- A new formation factor calculation model, called CWNM, is proposed. It can accurately and quantitatively describe the electrical conductivity of rocks with equations
- Through the comparison of 24 sets of experimental data on rock electrical properties, the CWNM evaluation model has demonstrated remarkable performance across various types of rocks and sediments, exhibiting strong adaptability

1 Introduction

The formation factor (abbreviated hereinafter as F) is one of the key parameters reflecting the characteristics of porous sediments and rocks; it is regarded as a basic reservoir property (Sen et al. 1981; Adler et al. 1992; Chen et al. 2019; Bakar et al. 2019; Zhou et al. 2022). Accordingly, this parameter is essential for oil and gas exploration and development (Soleymanzadeh et al. 2018; Esmaeilpour et al. 2021), geological carbon dioxide sequestration (CO_2) and hydrogen (H_2) storage (Vialle et al. 2014; He et al. 2017; Zhou et al. 2017; Rembert et al. 2020; Caesary et al. 2022; Hematpur et al. 2023) and hydrate identification (Constable et al. 2020; Ghanbarian and Male 2021; Stern et al. 2021; Pei et al. 2022). Given these applications, a highly precise method is needed to determine the formation factor and, by doing so, accurately estimate the permeability (Tang et al. 2017a; Sun and Wong 2018; Qiao et al. 2022) and saturation (Shahsenov and Orujov 2018; Rocha et al. 2019; Li et al. 2019) of that formation.

For rocks and sediments with a simple pore structure and high porosity, experimental methods are the most reliable approach for determining the formation factor, and of these techniques, rock-electric experiments are the most direct (Attia et al. 2008; Lee et al. 2021; Zhang et al. 2022). Rock-electric experiments used to reveal the formation factor measure the ratio of the resistivity of the brine-saturated rock (R_o) to the resistivity of the brine (R_w) (Permyakov et al. 2017; He et al. 2018; Mustofa et al. 2022). However, such experiments not only demand considerable time and labour but also have difficulty providing accurate resistivity estimates of tight, salt-saturated rocks, such as shales and tight sandstones (Wu et al. 2020; Liu et al. 2021; Zhu et al. 2021, 2022; Al-Mukainah et al. 2022). In addition, the pore structure of an unconsolidated sedimentary rock can easily change during the experiment (Jackson et al. 2002; Wang et al. 2020); the high capillary pressure due to the complex pore structure and small pore size also makes it difficult to complete rock-electric experiments on extremely tight rocks such as shale. More importantly, it is difficult to perform direct measurements on sediments and rock formations in-situ. As an alternative, the formation factor can also be obtained by combining the rock scanning method with engineering and computer-aided methods, such as finite element analysis (Sun et al. 2021; Wu et al. 2022). Unfortunately, these approaches are still quite expensive (Rahman et al. 2017; Liu et al. 2017; Yang et al. 2018; Jin et al. 2020).

Many scholars have sought the quantitative relationships between the formation factor and other characteristics of porous media (Cosenza et al. 2015; Mawer et al. 2015; Hakimov et al. 2019; Yang et al. 2022; Roozshenas et al. 2022). These studies have made it possible to indirectly calculate an accurate formation factor using geophysical methods (Cook

et al. 2012). Archie (1942) first proposed the generally accepted quantitative relationship (known as the Archie equation) between the formation factor and porosity in a high-porosity and high-permeability brine-saturated sandstone core, $F = \frac{R_o}{R_w} = \frac{a}{\varphi^m}$ where R_o refers to the resistivity of rocks saturated with brine, φ refers to the porosity, a is the tortuosity coefficient and m is the cementation factor. Among these variables, the m parameter may be a variable intermediate parameter (Qin et al. 2016; Zhou et al. 2019; Mahmoodpour et al. 2021). The Archie equation is currently the most widely used model. This approach does not consider the effect of surface conductivity. Surface conductivity is defined as the contribution of surface conductivity due to electrical conduction in nanoscale domains at the silica particle surface or at the fluid/particle interface (Revil and Glover 1998; Revil et al. 2014). Significant surface conductivities may occur in conductive minerals that are rich in smectites, illite clays (Waxman and Smits 1968; Greve et al. 2013) and pyrites (Clavier et al. 1976; Clennell et al. 2010) but are otherwise generally negligible. In order to simplify our statement, surface conductance will not be discussed here, but in fact many scholars have tried to solve the problem of surface conductance (Glover et al. 1994; Ruffet et al. 1995; Olsen et al. 2008; Bernabé et al. 2016).

Many low-porosity and low-permeability rocks and sediments with ultrahigh porosity have been found in various environments; these rocks do not meet the conditions required by the Archie equation (Yang et al. 2017; Lai et al. 2019; Siddiqui et al. 2020; Balsamo et al. 2020; Glover et al. 2020). Consequently, many types of methods have been developed to characterize the formation factor (Berg et al. 2022; Guo et al. 2021). The existing calculation models can basically be divided into 4 categories: (1) empirical models based on experimental measurements, which are aimed mainly at the selection of parameters m and a for different reservoirs (Winsauer 1952; Kennedy and Herrick 2012; Ghanbarian et al. 2014); (2) bound and mixing models, which take the form of multiple conducting phases, either in parallel or in series (Guéguen and Palciauskas 1994; Glover 2010, 2016; Pang et al. 2022); (3) pore network models, which are used to study the physical transport characteristics of rocks and provide an analytical solution for the formation factor based on an approximation model (Xiao et al. 2008; Bernabé et al. 2010; Bauer et al. 2011; Cai et al. 2017); and (4) theoretical models, which are cleverly based on the simplification of the pore space to deduce the model (Ellis et al. 2010; Yue and Tao 2013; Tang et al. 2015).

Theoretical models have the potential to characterize diverse types of porous rocks and sediments with abstract yet representative pore morphologies under correct and reasonable assumptions (Cai et al. 2017). Various theoretical models describing the formation factor–porosity relationship have been proposed (Kolah-kaj et al. 2021). A single abstract pore is commonly utilized to describe the conductivity characteristics of a rock (Carman 1937; Patnode and Wylie 1950; Li 1989; Wang and Zhang 2019). This model was the initial theoretical model. However, it remains difficult to characterize the formation factors of newly discovered increasingly complex porous rocks and sediments. Hence, many improved theoretical models have been proposed. The most common categorization divides theoretical models into 4 categories: (1) single capillary bundle models, (2) fractal models, (3) percolation and critical path analysis models and (4) effective medium approximations. In terms of single capillary bundle models, Revil et al. (1998) constructed a new electrical conductivity equation based on Bussian's model (Bussian 1983), which accounted for the special performance of ions in the pore space. Müller-Huber et al. (2015) developed a pore type with a varying cross-sectional area and set the pore cross-sectional area to change exponentially; Cai et al. (2019) subsequently extended this design. In addition, Hu et al. (2017) proposed a trapezoidal pore whose cross-sectional area change regularly and continuously.

For fractal models, Wei et al. (2015) proposed a rock formation factor calculation model that combines the electrical tortuosity fractal dimension and the pore fractal dimension. Thanh et al. (2019) suggested using minimum and maximum pore/capillary radii, the pore fractal dimension, and the tortuosity fractal dimension to comprehensively characterize formation factors. Liu et al. (2020) employed the normalized pore fractal dimension and normalized maximal pore diameter to predict the electrical properties of hydrate-bearing sediments and achieved good results. Effective medium theory has also been utilized. For instance, Han et al. (2015) developed a multiphase incremental model to characterize the formation factors of pyrite-bearing sandstones. Revil et al. (2018) found that the differential effective medium can be used to express the electrical characteristics of granular media. Hu et al. (2019) used effective medium theory to calculate the hydrate saturation of argillaceous sandstone. Another alternative is percolation theory, which was originally proposed by Kirkpatrick (1973). Gueguen and Dienes (1989) demonstrated the correlation between permeability and formation factors. Daigle et al. (2015) demonstrated that the formation factors of clay-rich sediments, due to their relatively wide pore distributions, can be expressed by percolation theory. Ghanbarian and Male (2021) theoretically explained and proposed a power-law relationship between the formation factor and permeability. Furthermore, Esmaeilpour et al. (2021) reported that formation factors can be further calculated for different pore throat distributions by using the theoretical equation for calculating permeability. A considerable amount of other research has been conducted on rock conductivity based on percolation theory (Hunt 2004; Ghanbarian et al. 2013).

Even if a model based on a single abstract pore could reflect the actual microscopic characteristics of partial porosity, it would be difficult to characterize the entire pore space with strong heterogeneity in this way (Wang 2018; Zambrano et al. 2021). This difficulty limits the use of theoretical models in rocks with complex pore structures. Dividing the pore space of a porous medium into a combination of multiple pores both in series and in parallel may allow researchers to better characterize the effect of an actual porous medium's pore space on its conductivity. To the best of our knowledge, these models have not been classified into a specialized category in previous studies. Such models should actually be called v) multiple-pore theoretical models, belonging to new category in theoretical models. For example, the equivalent rock element model (EREM) is a typical multiple-pore theoretical model (Shang et al. 2003). The EREM divides the pore system into pores along the potential gradient and pores perpendicular to the potential gradient, with differences in the ability of the brine to conduct electric current in the 2 types of pores. Li et al. (2012) proposed a dual pore saturation model that regards the total resistance of the rock as the resistances of movable water and irreducible water (the latter includes clay-bound water and microcapillary pore water) in parallel. The microcapillary pore water content is also often considered separately, such as the dual mineral model (Brown 1986, 1988) and conductive rock matrix model (Givens 1987). Models with similar ideas include the three-water model and the new three-water model, both of which regard a rock's conductive channel as free fluid water, micropore water and clay-bound water both in series and in parallel (Mo et al. 2001; Zhang et al. 2010a, b; Fu and Wang 2022). Furthermore, Iheanacho (2014) established a formation factor model that considers various pore types in argillaceous sandstone by taking into account the differences in electrical conductivity among various types of pores in the argillaceous matrix skeleton. Piedrahita and Aguilera (2017) proposed a formation factor model that considers the conductivity differences between fractures and pores for fractured rocks. In contrast with the above models, whose classification criteria are based on the pore type (Tian et al. 2020; Tariq et al. 2020), Liu et al. (2013) proposed a sphere–cylinder model to describe the conductivity characteristics of tight reservoirs using spheres and cylinders to represent pores and throats, respectively. Wang and Zhang

(2019) also proposed a pore space segmentation method with a greater number of potential pore structure assumptions, and Li et al. (2017) and Meng and Liu (2019) also proposed similar conceptual models.

Multiple-pore theoretical models' scheme has strong ability to characterize the conductivity characteristics of rocks displaying non-Archie behaviours in practical applications (that is, in the entire porosity range, the distributions of the formation factor and porosity are not exactly the same as those specified by the Archie equation) (Shang et al. 2003); this benefits from its adaptability to complex porous media. It is essential to correctly abstract the pores even with multiple-pore theoretical models. At present, multiple-pore theoretical models mainly divide the entire pore space according to either pore types (Liu et al. 2018) or pore throat differences (Liu et al. 2013; Ghanbarian et al. 2017; Li et al. 2017; Meng 2018; Meng and Liu 2019; Wang and Zhang 2019). All different components are connected either in series or in parallel. However, such division is not necessarily suitable for all types of porous rocks. For example, many multiple-pore theoretical models simulate the pore space as a combination of pores and throats, but pores and throats are also abstractions utilized to divide the pore space based on the rock's hydraulic conductivity characteristics, the resulting model is true only if the seepage properties of the rock are completely consistent with its conductivity properties, but this topic continues to be a subject of debate with no definitive answer (Berg and Held 2016; Li and Hou 2019); in other words, pore size is not the only factor that determines the resistivity (Stenzel et al. 2016; Ghanbarian et al. 2017; Rembert et al. 2020; Sun et al. 2021). Moreover, multiple-pore theoretical models based on pore types are sometimes problematic, as different types of pores may also have the same conductivity characteristics when their pore shapes are similar.

In this work, a new electrical conductivity model for porous media is proposed; multiple-pore theoretical models are supplemented. The entire pore space is divided into nonconductive pores, weakly conductive pores and conductive pores, and the conductive pores are designed as truncated cone pores. Then, the model developed in the present work is compared with the available experimental data for different types of porous rocks, and the results confirm our model's strong tolerance and broad scalability. Finally, where to use the model is suggested and future directions of development are discussed.

2 Methodology

2.1 Classic Capillary Bundle Model

The capillary bundle model is a typical ideal theoretical model (Cheng et al. 2017) that is usually used to describe the electrical conductivity and seepage characteristics of rocks (Watanabe and Flury 2008). In the capillary bundle model, as in all capillary models, L, L_w, S and S_b represent the length of the rock, the length of the capillary bundle pores in the rock, the cross-sectional area of the rock and the cross-sectional area of the capillary bundle pores in the rock, respectively. According to the parallel connection of rocks and pores, it yields:

$$\frac{1}{r_o} = \frac{1}{r_{ma}} + \frac{1}{r_w} \tag{1}$$

where r_o, r_{ma} and r_w represent the resistance of the rock, the skeleton and the formation water, respectively.

Because the skeleton does not participate in the electrical conduction of the rock in the usual case, $r_{ma} \to +\infty$. Therefore, incorporating Ohm's law yields the following equation:

$$R_o \frac{L}{S} = R_w \frac{L_w}{S_b} \tag{2}$$

The pores are curved, and the current conduction path during electricity conduction is also curved. τ_e is a parameter indicating the degree of bending. L_w is the product of τ_e and L, and $S_b = \frac{S\varphi}{\tau_e}$. Equation (2) can be simplified as:

$$\frac{R_o}{R_w} = \frac{SL_w}{S_b L} = \frac{\tau_e^2}{\varphi} \tag{3}$$

Equation (3) constitutes the basic equation for predicting the formation factor in a variety of theoretical and semiempirical models (Paterson 1983; Walsh and Brace 1984). In addition, the capillary bundle model can also integrate pore bodies and pore throats (Ghanbarian et al. 2017; Cai et al. 2019; Wang and Zhang 2019). But as mentioned above, the variety of complex porous media may be difficult to be fully solved by single capillary bundle models.

2.2 Truncated Cone Pore in Porous Media

Hu et al. (2017) believed that for pores with different cross-sectional areas, starting from the conductivity theory of porous media, the current conduction path of the pores can be regarded as composed of a large number of capillaries with variable cross-sectional areas. When conducting electricity, the resistance of the variable-section capillary is composed of a large number of resistance microelements connected in series. Then, the connection order of any resistance microelements can be adjusted, and the microelement cross-sectional area can be arranged from large to small. On a two-dimensional plane, the rearranged equivalent capillary is a trapezoid, and thus, the concept of trapezoidal pores is proposed (detailed description of the concept with schematic details in Section 3.1 of Hu et al. 2017). Hu et al. (2017) also demonstrated the effectiveness of this idea in actual rocks.

Along this line of thinking, this paper reviews and reconsiders the pore as a volume concept. It should not be called a trapezoidal pore, using the concept of a truncated cone to characterize the conductive pore. The top and bottom surfaces of this shape are circular, similar to a cone cut-off by a plane parallel to the bottom. Similar to a cylinder, the truncated cone also has a shaft, a base, sides and a generatrix (Fig. 1).

The cross section of a pore is approximated as circular; it is a common assumption (Müller-Huber et al. 2015; Hu et al. 2017; Li et al. 2017). The corresponding model derivation process is described in Appendix 1; the resistance of such pores is:

$$r_g = \int_0^{L_g} R_w \frac{\mathrm{d}l}{S(l)} = \frac{R_w L_g}{\pi c_2 r_{\min}^2} \tag{4}$$

In the above equation, dl indicates that l is the integral variable of the pore length to be integrated, and its range is 0-L_g; r_g characterizes the resistance of a single truncated cone pore when saturated with water, and it can be determined via integration over the pore; L_g refers to the pore length; c_2 is the pore scaling factor, which represents the area ratio of the pore with the widest cross-sectional area to the pore with the narrowest cross-sectional area among the truncated cone pores; and $r_{\min}$ represents the minimum radius of a truncated

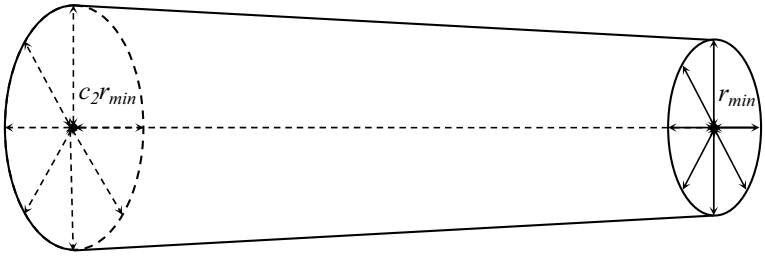

Fig. 1 Schematic of the truncated cone pore and the corresponding descriptive parameters

cone pore. A single pore can be characterized by using the abovementioned truncated cone pore.

2.3 Characterization of Pore System Electrical Conductivity

2.3.1 Influence of Pore Structure Complexity

The classification of the entire pore space in multiple-pore theoretical models is particularly important. In conjunction with the introduction, this paper does not simply classify pores by the pore type or pore throat characteristics but instead applies a more general pore space classification that can be adapted to calculate the formation factor. We can consider the impacts of complex pore structures from another perspective, including extreme cases. If the pore structure does not have any effect on conductivity, since the salinity of pore water is consistent, the conductivity of all pores is the same. In other words, regardless of how complex the actual pore space characteristics of porous media are, the final impact on the conductivity of the pore space leads to differences in the conductivity of pores at different locations.

Therefore, according to the influence of the pore structure complexity on rock pore conductivity, the pore conductivity can be discussed and directly classified, and the corresponding electrical conductivity model can be established. The model can theoretically be applied to all types of porous media with complex pore structures. In the characterization method of rock permeability, a similar pore classification concept according to the effect of different positions of pores on permeability is also proposed (Nishiyama and Yokoyama 2017).

When under the influence of diagenesis, and when some pores that are not in the main conductive channel appear, the conductivity of those pores is reduced. Since ignoring the effects of these pores can introduce errors into the prediction of the formation factor, their contribution to the rock conductivity should be considered separately. These affected pores are referred as weakly conductive pores.

Since the complexity of the pore structure reduces the conductivity of some pores, this complexity can also prevent ions in some pores from moving in the direction of the electric field. These pores are refereed as nonconductive pores. These pores may become completely removed from the connected pore network, or they may be too far from the main conductive channel. It is worth mentioning that if a laboratory uses the fluid injection method for porosity determination, the nonconductive pores should originate only from interconnected pores rather than dead pores.

Thus, the entire pore system can be divided into conductive pores, weakly conductive pores and nonconductive pores. These pores should appear abundantly in porous rocks and sediments, and their proportions may be related to the complexity of the pore structure. Numerical simulations and experiments in some recently published papers seem to validate our model. For instance, the simulation results in Berg et al. (2022) suggest that even for rocks with a simple pore structure and high porosity, the electric field distribution in the pore space is still affected by the shapes of the particles, resulting in heterogeneous electrical conductivity among pores at different positions. Sun et al. (2021) similarly reported that the current field distribution is not uniform even at the pore scale and is related to the pore size distribution. Feng et al. (2022) used finite element simulations to find significant differences in the current density of pores at different locations in a 3D digital core. Weakly conductive pores should theoretically be associated with nonconductive pores, and both exist in the pore system where the pore distribution is more complex. Moreover, with the deepening of diagenesis, the pore structure is further deteriorated, and it may happen that the conductive pores in the position with complex pore distribution are converted into weakly conductive pores, and the weakly conductive pores are converted into nonconductive pores.

2.3.2 Formation Factor Expression

Since the main reason for the difference in conductivity between weakly conductive pores and nonconductive pores is the difference in their distance from the main conductive channels, there is no fundamental difference between these 2 types of pores in terms of their origin and they are also associated. Therefore, when forming an abstract pore space, a contact between weakly conductive pores and nonconductive pores is designed (when porosity does not include sources of dead pores). The weakly conductive pores and the nonconductive pores are not located in the mainstream conductive channel but are located at the relative boundaries or corners of the pore network. Due to the complexity of the pore network, the characteristic parameters of different conductive pores are inconsistent; the pore space of the entire rock should be abstracted into a collection of multiple pores. When determining the equivalent conductive electrical circuit, weakly conductive pores should be connected in series with conductive pores, and all conductive pores should be connected in parallel. Moreover, the conductive pores are set as the truncated cone pores, meaning that the assumptions of Eq. (4) are valid for conductive pores, whereas all other pores are still regarded as capillary bundles with a constant pore cross-sectional area, and they are still tortuous. This setting also maximizes the accuracy with which the rock's electrical conductivity is characterized while minimizing the increase in the number of parameters. Ultimately, conductive pores occupy a considerable percentage regardless of whether the pore structure is complex, while weakly conductive pores and nonconductive pores do not occupy the main channel, and the correct characterization of conductive pores is the most important.

Suppose that the length of the rock is L and the cross-sectional area is S. The length of the conductive pores is denoted as L_1, and the cross-sectional area is S_1. The lengths of weakly conductive pores and nonconductive pores are L_2 and L_3; the cross-sectional area of weakly conductive pores is S_2 and that of nonconductive pores is S_3.

The following settings are associated with the above parameters. Among them, some parameters are set: e characterizes the ratio of L_2 to L_1, and c_1 characterizes the ratios among S_1, S_2 and S_3:

$$L_2 = eL_1 \tag{5}$$

$$S_2 + S_3 = c_1 S \tag{6}$$

$$S_2 = c_1 c_3 S \tag{7}$$

$$\frac{L_1 + L_2}{L} = \frac{(1+e)L_1}{L} = \tau_e \tag{8}$$

In the above equations, c_1 refers to the ratio of the sum of the cross-sectional areas of weakly conductive pores and nonconductive pores to the cross-sectional area of the entire rock, c_3 refers to the ratio of the cross-sectional area of weakly conductive pores to the sum of the cross-sectional areas of weakly conductive pores and nonconductive pores, and τ_e refers to the tortuous conductivity of the pore space. The entire pore possesses only one τ_e, whose value is determined by combining L_1 and L_2, L_3 does not be added because the corresponding pores are not conductive.

Then, according to Fig. 2b and the law of resistance, the resistivity of the entire rock saturated with water is as follows:

$$R_o = r\frac{S}{L} = \left(\left(\sum_{j=1}^{N} \frac{1}{r_{1j}}\right)^{-1} + r_2\right)\frac{S}{L} \tag{9}$$

where N is the number of conductive pores according to the assumption of multiple truncated cone pores, r_{1j} refers to the resistance of the j-th conductive pore and r_2 refers to the resistance of weakly conductive pores.

According to the law of resistance, combining Eqs. (6) and (8), the resistance of weakly conductive pores can be characterized as follows:

$$r_2 = R_w \frac{L_2}{S_2} = \frac{R_w e \tau_e}{(1+e)c_1 c_3}\frac{L}{S} \tag{10}$$

In a total of N conductive pores, some conductive pores may have the same characteristic parameters. Assuming that there are O-type conductive pores with different characteristic parameter, combined with Eq. (4), then the following equation applies:

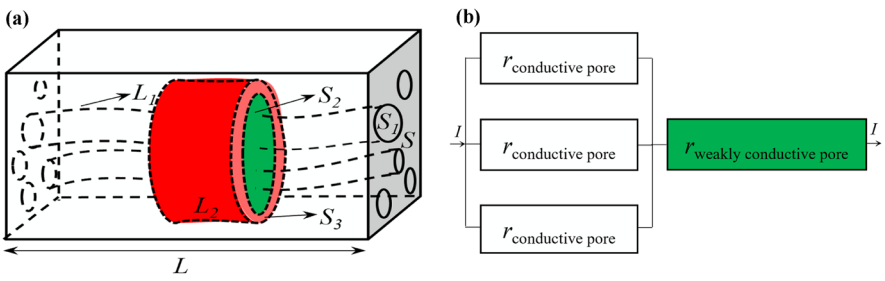

Fig. 2 Schematic diagram related to the derivation process of the model

$$\left(\sum_{j=1}^{N}\frac{1}{r_{1j}}\right)^{-1}=\left(\sum_{j=1}^{N}\frac{1}{\frac{R_wL_{1j}}{\pi c_{2j}r_{\min j}^2}}\right)^{-1}=\frac{R_wL_1}{\pi}\left(\sum_{i=1}^{O}F_ic_{2i}r_{\min i}^2\right)^{-1} \tag{11}$$

where F_i is the number of corresponding truncated cone pores of i-th type whose radii and pore scaling factors are denoted $r_{\min i}$ and c_{2i}, respectively. The total number of categories of all pores after classification according to the difference in $r_{\min}$ and c_2 is $O<N$.

According to Eqs. (9)–(11), the total resistance is expressed as follows:

$$r=\left(\sum_{j=1}^{N}\frac{1}{r_{1j}}\right)^{-1}+r_2=\frac{R_wL_1}{\pi}\left(\sum_{i=1}^{O}F_ic_{2i}r_{\min i}^2\right)^{-1}+\frac{R_we\tau_eL}{(1+e)c_1c_3S} \tag{12}$$

Note that, however, reclassification of all conductive pores according to the characteristics of c_2 and $r_{\min}$ results in $O<N$. However, in fact the total number of capillaries of conductive pores is still certain, so here it is:

$$\sum_{j=1}^{N}F_j=\sum_{i=1}^{O}F_i \tag{13}$$

Combined with Eqs. (5)–(13), then the formation factor can be characterized as follows:

$$F=\frac{R_o}{R_w}=r\cdot\frac{S}{LR_w}=\frac{\tau_eS}{\pi(1+e)\sum_{j=1}^{N}F_j}\left(\frac{\sum_{i=1}^{O}F_ic_{2i}r_{\min i}^2}{\sum_{i=1}^{O}F_i}\right)^{-1}+\frac{e\tau_e}{(1+e)c_1c_3} \tag{14}$$

Equation (14) can be characterized as Eq. (15), and the intermediate process of conversion is shown in Appendix 2.

$$F=\frac{\tau_e^2}{(1+e)^2}\frac{\overline{r_m}^2L_1}{\varphi_pL}\frac{1}{c_2\overline{r_m}^2P}+\frac{e\tau_e}{(1+e)c_1c_3} \tag{15}$$

where φ_p refers to the porosity of all truncated cone pores, that is, the porosity of the conductive pores. P refers to the ratio between the radius of the minimum and average circular pore cross-sectional area. Furthermore, by substituting φ_p and P, the final formation factor expression can be obtained (Eq. (16)), and the derivation process of this expression is shown in Appendix 3. In Appendix 3, the assumption of $L_2\approx L_3$ is used, which reduces one parameter of the model. A discussion of the impact of such settings on the model is given in Appendix 4.

$$F=\frac{\left(c_1\tau_e+c_1c_3e_{ps}\tau_e-\varphi\right)^2\left(1+c_2+c_2^2\right)}{3c_1^2c_2c_3e_{ps}\left(1+c_3e_{ps}\right)}\frac{1}{\varphi}+\frac{\varphi}{\left(1+c_3e_{ps}\right)c_1^2c_3} \tag{16}$$

This shows that the theoretical relationship between the formation factor and porosity may be more complex than the empirical relationship shown by Archie's equation. The proposed model reveals that to determine the conductivity properties of extremely complex porous media, 5 parameters should be determined. It refines these potential factors that affect the conductivity insomuch that, theoretically, the model can describe many types of complex porous media. Because the proposed model is composed of conductive pores,

weakly conductive pores and nonconductive pores, our model is called the conductive pores + weakly conductive pores + nonconductive pores model (CWNM).

3 Sensitivity Analysis of the CWNM

According to Eq. (16) for calculating the formation factor established in this paper, the formation factor is related to c_1, c_2, c_3, e_{ps} and τ_e. To further analyse the influence of these parameters that reflect the rock's pore conductivity characteristics on the formation factor and whether there is any overlap between the parameters in terms of pore information, Fig. 3 shows the relationship between the formation factor and porosity under different values of c_1, c_2, c_3, e_{ps} and τ_e.

As shown in Fig. 3, the formation factor and porosity are controlled within a range of common values. When other factors are fixed, c_1, c_2 and τ_e are positively correlated with the resistivity of the rock, while c_3 and e_{ps} are negatively correlated. Moreover, the influence of each parameter on the formation factor is unique. Among them, c_1 is an obvious parameter that affects non-Archie behaviour, which shows that nonconductive pores and weakly conductive pores are the key to produce non-Archie behaviour and affect its level. The c_3 and e_{ps} also have a certain ability to control non-Archie behaviour. These parameters also come from nonconductive pores and weak conductive pores.

The c_2 parameter reflects the structural characteristics of conductive pores, especially their heterogeneity. Figure 3b shows that with a linear change in c_2, the change shown in the figure is also basically linear when both coordinate axes are logarithmic. c_2 has little effect on the slope of the formation factor–porosity relationship. As c_2 changes, as shown in the figure, the formation factor–porosity relationship lines are parallel.

The c_3 parameter can indicate the proportion of weakly conductive pores among the total porosity affected by the pore structure. According to Eq. (49), c_3 reflects the proportion of weakly conductive pores occupying the sum of weakly conductive pores and nonconductive pores. This parameter further refines the conductivity of the pores. The smaller the c_3, the more obvious its change has on the formation factor; when nonconductive pores proportion gradually increases, the formation factor rapidly increases; hence, the impacts of weakly conductive pores and nonconductive pores on the formation factor are different. This pattern also illustrates the considerable importance of distinguishing between nonconductive pores and weakly conductive pores.

The e_{ps} parameter characterizes the effect of the transition from conductive pores to weakly conductive pores on the formation factor when the pore structure is complex. As the pore structure becomes more complicated, e_{ps} decreases, and a change in the e_{ps} affects the formation factor. This effect can explain why the pore structure is so pertinent to understanding the changes in the low-porosity reservoir formation factor: the more complex the pore structure is, the greater the impact on the reservoir. In addition, the e_{ps} and c_3 parameters are similar, as both produce effects over the entire range of the actual porosity.

In addition, the effect of τ_e on the formation factor–porosity relationship should also be considered, as shown in Fig. 3e. τ_e is often selected in models because its influence on the formation factor may be nearly ubiquitous (Abderrahmene et al. 2017; Sevostianov et al. 2017; Xu and Jiao 2019; Lala 2020; Fu et al. 2021; Silva et al. 2022). In theory, τ_e must be > 1 to conform to the theoretical setting, and the range of this parameter is set in a targeted manner in the subsequent optimization inversion.

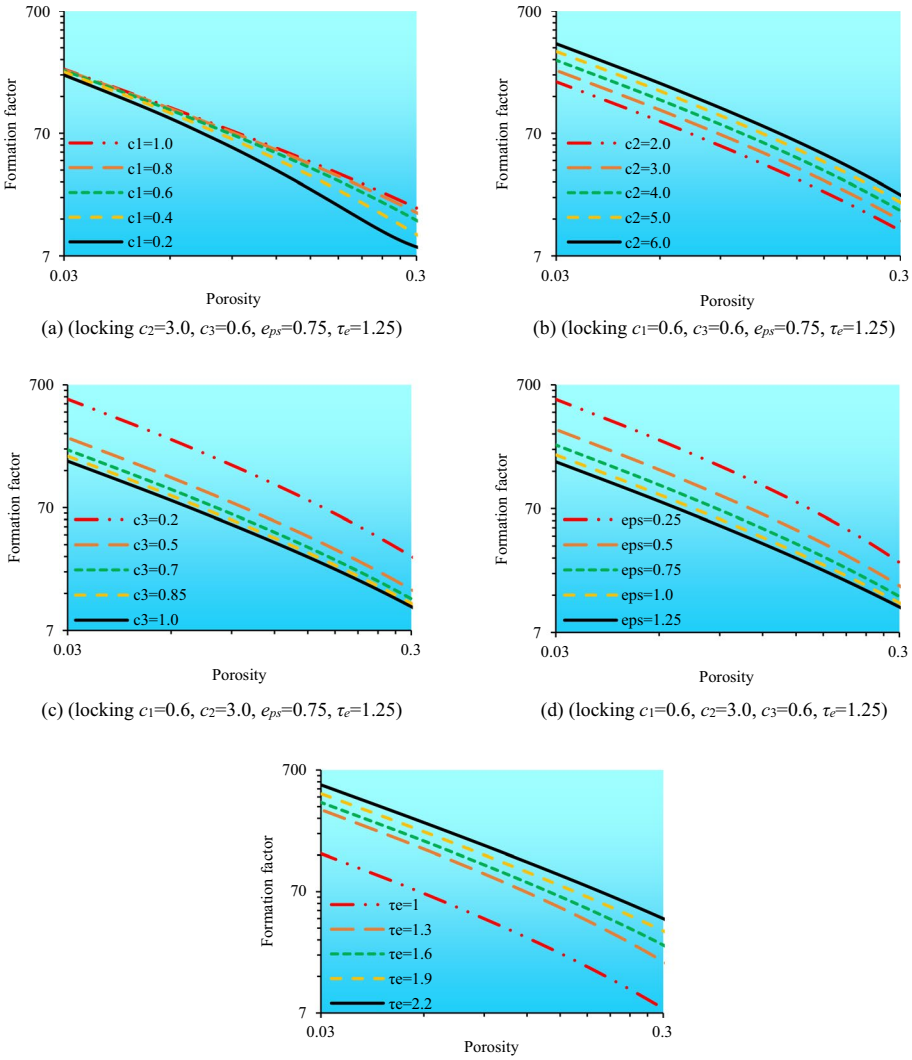

(a) (locking c_2=3.0, c_3=0.6, e_{ps}=0.75, τ_e=1.25)

(b) (locking c_1=0.6, c_3=0.6, e_{ps}=0.75, τ_e=1.25)

(c) (locking c_1=0.6, c_2=3.0, e_{ps}=0.75, τ_e=1.25)

(d) (locking c_1=0.6, c_2=3.0, c_3=0.6, τ_e=1.25)

(e) (locking c_1=0.6, c_2=3.0, c_3=0.6, e_{ps}=0.75)

Fig. 3 Changes in each key parameter in the CWNM and their effect on the formation factor–porosity relationship

4 Explanation of Differences by Comparing Existing Formation Factor Models

The theoretical advances offered by the CWNM should be analysed. In this section, 6 models for evaluating the formation factor are introduced for comparison, including 3 single capillary bundle models (the capillary bundle model, trapezoidal pore model (TPM) (Hu et al. 2017), and capillary channel model (CCM) (Müller-Huber et al. 2015) and 3 multiple-pore theoretical models (the EREM (Shang et al. 2003), pore throat model (PTM) (Li

et al. 2017), and Meng and Liu model (Meng and Liu 2019), which were utilized to theoretically explore the differences between these models and the proposed model.

4.1 Comparison with Existing Single Capillary Bundle Model

4.1.1 Capillary Bundle Model

The main difference between the capillary bundle model and the CWNM is that the proposed model takes into account variations in the pore cross-sectional area, and the influence of pore conductivity characteristics is controlled by c_2 in Eq. (16). The parameters c_1, c_3 and e_{ps} control the characteristics of various pore ratios; likewise, these settings do not exist in the capillary bundle model. When c_2 has a value of 1 and e_{ps} approaches infinity, the values of c_1 and c_3 are not important, and Eq. (16) degenerates into Eq. (3), whereas the proposed model can characterize the final influence of a complex pore structure on any rock/sediment and thus is more versatile.

$$\lim_{c_2\to 1, e_{ps}\to+\infty} F = \lim_{c_2\to 1, e_{ps}\to+\infty} \frac{\left(c_1\tau + c_1c_3e_{ps}\tau_e - \varphi\right)^2\left(1 + c_2 + c_2^2\right)}{3\left(c_1^2c_2c_3e_{ps}\left(1 + c_3e_{ps}\right)\right)}\frac{1}{\varphi} + \frac{\varphi}{\left(1 + c_3e_{ps}\right)c_1^2c_3} = \frac{\tau_e^2}{\varphi} \tag{17}$$

4.1.2 Trapezoidal Pore Model (TPM)

The TPM assumes that the pores in a rock or sediment can be modelled as a series of trapezoidal pores (Hu et al. 2017). This model considers the influences of not only changes in the cross-sectional areas of pores but also changes in the tortuous conductivity of the pores on the conductivity characteristics of the entire rock. Through these assumptions, the formula for calculating the formation factor derived in the TPM is:

$$F = \frac{\tau_e^2}{P_t\varphi} \tag{18}$$

where P_t is called the trapezoidal factor and its calculation equation is:

$$P_t = \frac{r_{\max}r_{\min}}{r_{\text{ave}}^2} \tag{19}$$

where $r_{\max}$ refers to the largest pore radius, $r_{\min}$ refers to the smallest pore radius, and r_{ave} refers to the average pore radius of trapezoidal pores. P_t reflects the homogeneity of the cross-sectional area of the trapezoid pores, similar to the information represented by the c_2 parameter set in the model in this paper. Equations (18) and (4) show that although the TPM has increased the influence of the change in the pore cross-sectional area, the influence of P_t on the formation factor is more analogous to a coefficient. There are some similar formation factor expressions, and the expressions they give are the product of pores and multiple coefficients, without addition and subtraction between parameters (Herrick and Kennedy 2009; Xie et al. 2022). If the proposed model does not consider weakly

conductive pores and nonconductive pores, since the assumptions are similar, Eq. (18) can be derived.

4.1.3 Capillary Channel Model (CCM)

Müller-Huber et al. (2015) considered the influence of pore cross-sectional area on conductivity. They used the following function to model the variation in the pore radius:

$$r(l) = r_t e^{\alpha l}, \quad \alpha = \frac{1}{L}\ln\frac{r_b}{r_t} \tag{20}$$

where $r(l)$ refers to the corresponding radius value at pore length l, r_t refers to the pore throat radius, α refers to the pore shape factor and r_b refers to the pore body radius. The corresponding formation factor expression is as follows:

$$F = \frac{\left(1-\left(\frac{r_t}{r_b}\right)^2\right)\left(\left(\frac{r_b}{r_t}\right)^2-1\right)}{\left(2\ln\frac{r_b}{r_t}\right)^2\varphi} \tag{21}$$

No multiple pores are added to the TPM assumption, resulting in a single conductivity that can be characterized. The difference in assumptions about the pore size change of the cross-sectional area is the biggest difference between the proposed model and the CCM, and the pore size change designed in this paper is linear rather than exponential. In the proposed model, when the change in pore size conforms to the CCM settings in Eq. (16), and when weakly conductive pores and nonconductive pores are not considered, given the assumptions based on the CCM, Eq. (21) can be obtained by derivation.

4.2 Comparison with the Existing Multiple-Pore Theoretical Models

4.2.1 Equivalent Rock Element Model (EREM)

In the EREM, the rock is considered a regular cylinder composed of pore volumes P_f, parallel pore volumes P_p and skeleton volumes, all of which (differing in size) are connected in series to form the conductive system of the whole rock (Shang et al. 2003). Assume that the ratio between these 2 types of pores is C, which is called the pore structure efficiency. The role of the C parameter is similar to the definition of the e_{ps} parameter in this paper, and the corresponding expression is:

$$C = \frac{P_f}{P_p} \tag{22}$$

Through a series of derivations, the expression for computing the formation factor based on the EREM is finally obtained:

$$F = \frac{(1-\varphi)^2}{C\varphi} + \frac{1}{\varphi} \tag{23}$$

Theoretically, compared to the EREM, the CWNM considers the influence of nonconductive pores, variation in pore cross-sectional area and tortuous conductivity on the formation factor. As shown in Sect. 3, the corresponding parameters have remarkable influences on the formation factor. If some elements are ignored, it is easy to obtain Eq. (23) using Eq. (16) when following the model derivation idea of EREM.

4.2.2 Pore Throat Model (PTM)

The PTM simplifies a real reservoir rock into a cube of unit volume and describes the complex pore structure as a pore network model composed of pores and throats. Li et al. (2017) assumed that the ratio of the throat radius (abbreviated r_c) to the pore radius (abbreviated r_s) can be denoted by the R_x parameter:

$$R_x = \frac{r_c}{r_s} \tag{24}$$

The expression equation of the formation factor can be given as follows:

$$F = \frac{\rho_o}{\rho_w} = \tau_e \frac{1 - 2r_s\sqrt{1 - R_x^2}}{\pi R_x^2 r_s^2} + \frac{1}{\pi r_s} ln \frac{1 + \sqrt{1 - R_x^2}}{1 - \sqrt{1 - R_x^2}} \tag{25}$$

The corresponding porosity expression is as follows:

$$\varphi = \left(\frac{2\pi}{3}\sqrt{1 - R_x^2}\left(2 + R_x^2\right) - 2\tau_e \pi R_x^2 \sqrt{1 - R_x^2} \right) r_s^3 + \tau_e \pi R_x^2 r_s^2 \tag{26}$$

In the PTM, to facilitate the actual measurement of the pore structure parameter, the pore throat ratio and the corresponding parameters are assumed. R_x is the reciprocal of the pore throat ratio, which is a pore structure parameter that can be obtained through experiments such as constant-rate mercury intrusion (Jiao et al. 2020). Therefore, the model essentially considers 2 different types of pores.

Compared with the CWNM, the PTM is different in two ways. The first is that the PTM does not consider the influence of changes in the pore cross-sectional area on the overall conductivity. Second, the PTM divides the pores into 2 types based on the difference between pores and throats. Throats reduce the efficiency with the current that is transmitted. Hence, the PTM and the CWNM consider all pores to be in series with other types of pores. This setting is similar between the two models.

4.2.3 Meng and Liu Model

Meng and Liu (2019) recently proposed a novel conductivity model in which the entire pore space is assumed to consist of 3 types of pores, namely, large pores, horizontal throats and vertical throats.

The horizontal throat–pore radius ratio and vertical throat–pore radius ratio are two parameters set in the model, and these parameters can be expressed as follows:

$$C_{d1} = \frac{R_{c1}}{R_s} \tag{27}$$

$$C_{d2} = \frac{R_{c2}}{R_s} \tag{28}$$

where R_{c1} refers to the throat radii in the horizontal directions and R_{c2} refers to the throat radii in the vertical directions. *Rs* refers to half of the side length of the large pore (set as a square pore). After the model is derived, the corresponding formation factors and porosity expressions are as follows:

$$\varphi = 8R_s^3 + 4\left(1 - 2R_s\right)R_s^2\left(C_{d1}^2 + C_{d2}^2\right) \tag{29}$$

$$F = \frac{1 - R_s}{4R_s^2C_{d1}^2} + \frac{1 - C_{d2}}{2R_s} + \frac{C_{d2}}{2R_s + C_{d2}\left(1 - 2R_s\right)} \tag{30}$$

In Eq. (30), the formation factor can be characterized by C_{d1}, C_{d2} and R_s. From this expression, the Meng and Liu model accumulates multiple terms whose model form is able to approximate non-Archie behaviours. Therefore, there are no nonconductive pores in this model; rather, there are 2 types of throats with different electrical conductivities. In addition, the tortuous conductivity parameter is not set in this model. Equation (16) in this paper is different under the assumption of different pores, so it is impossible to derive Eq. (30), but the effect of a change in e_{ps} on the formation factor–porosity relationship is similar to the effects of changes in C_{d1} and C_{d2}.

5 Results

In this section, the formation factor prediction effect of the CWNM is evaluated. One of the 3 multiple-pore theoretical models is selected, the EREM (Shang et al. 2003), and one of the 3 single capillary bundle models, the CCM (Müller-Huber et al. 2015), to compare differences in effects between models. The formation factor formulas of the EREM and CCM are shown in Eqs. (23) and (21), respectively. In addition, since the published literature does not provide the porosities of pores with different conductivities, it is difficult to explain how to obtain the parameters in the model through the results of previous simulations or experiments. Hence, an optimization method, namely a genetic algorithm, is used to obtain the parameters in the model (Holland 1975), as the use of optimization to determine the parameters of the formation factor calculation formula is a common statistical approach (Pan et al. 2016; Mahmoodpour et al. 2021). In Discussion section, potential methods for determining the model parameters are discussed.

The corresponding optimized objective function is:

$$f\left(c_1, c_2, c_3, e_{ps}, \tau_e\right) = \min\left(\sum_{m=k}^{M}\left(F_m - F_p\right)\right) \tag{31}$$

Equation (31) indicates that the criterion for determining the model parameters is mainly the accuracy. Note that for the EREM and CCM, Eq. (31) also be used to determine the optimal model parameters, namely, $\min\left(\sum_{m=k}^{M}\left(F_m - F_p\right)\right)$. For the parameters of the genetic algorithm, we set the crossover probability to 0.95, the mutation probability to 0.08 and the loop algebra to 500, which can ensure that our solution is reliable.

In the equation, min is the minimum value. m represents the m-th sample, M represents the total number of samples of a certain formation factor, F_m represents the actual formation factor measured experimentally, and F_p represents the estimated formation factor. In addition, the mean relative error (MRE) is used to characterize the accuracy, and the corresponding equation is:

$$\mathrm{MRE} = \frac{\sum_{m=k}^{M}\left(\frac{F_m - F_p}{F_m}\right)}{M} \tag{32}$$

In the experimental data presented below, their porosity was basically obtained by the fluid injection method. This ensures that the porosity results do not contain the porosities of dead pores, that is, the formation of nonconductive pores only relies on a complex interconnected pore system.

5.1 Conventional Medium- to High-Porosity Sandstone

In Sect. 5.1, the application effect of the CWNM in medium- to high-porosity sandstone is explored first. Three sets of data from higher-porosity sandstone, such as Bentheimer quarried sandstone, are selected here. The porosity and formation factor ranges of the 3 sets of data are 5.06–24.68% and 13.303–176.553 (Øren et al. 1998), 7.5–35% and 9.285–100.705 (Krohn and Thompson 1986), and 3.58–11.61% and 7.22–444.55 (Thompson et al. 1987). Figure 4 reveals the performance of the CWNM, EREM, and CCM on the 3 datasets. Based on these large amounts of data, we can analyse the proposed model functionality from multiple perspectives, such as the prediction effect of the formation factor prediction, the prediction differences among the 3 models and the ranges of the parameters. The trends of the 3 sets of data are examined, revealing obvious non-Archie behaviours (Shang et al. 2003). Figure 4a–c shows that the core data conform to the Archie equation when the porosity is high (greater than 8%); however, when the porosity is less than 8%, the relationship between the formation factor and porosity is different from that when the porosity is greater than 8%. Similar patterns were found in some other published papers, with corresponding porosity limits of 8%-10% (Zhang et al. 2016a). Specifically, for medium–high-porosity sandstone reservoirs, if the lower limit of the porosity of the reservoir is much greater than 8%-10%, the formation factor can be reliably calculated directly by using the Archie equation.

Next, the performance of the CWNM in the conventional medium–high-porosity sandstone is analysed. From the perspectives of the accuracy and prediction effect, the CWNM can adapt to conventional medium–high-porosity sandstone and can effectively approximate the experimentally measured formation factor. It is worth mentioning that the CWNM can accurately calculate the formation factors of data not only with porosities greater than 8% but also with porosities of less than 8% without changing the parameters. From a data point of view, this demonstrates that the CWNM can reflect the real rock conditions based on the reasonable division of the pore space. When rocks have similar properties and come

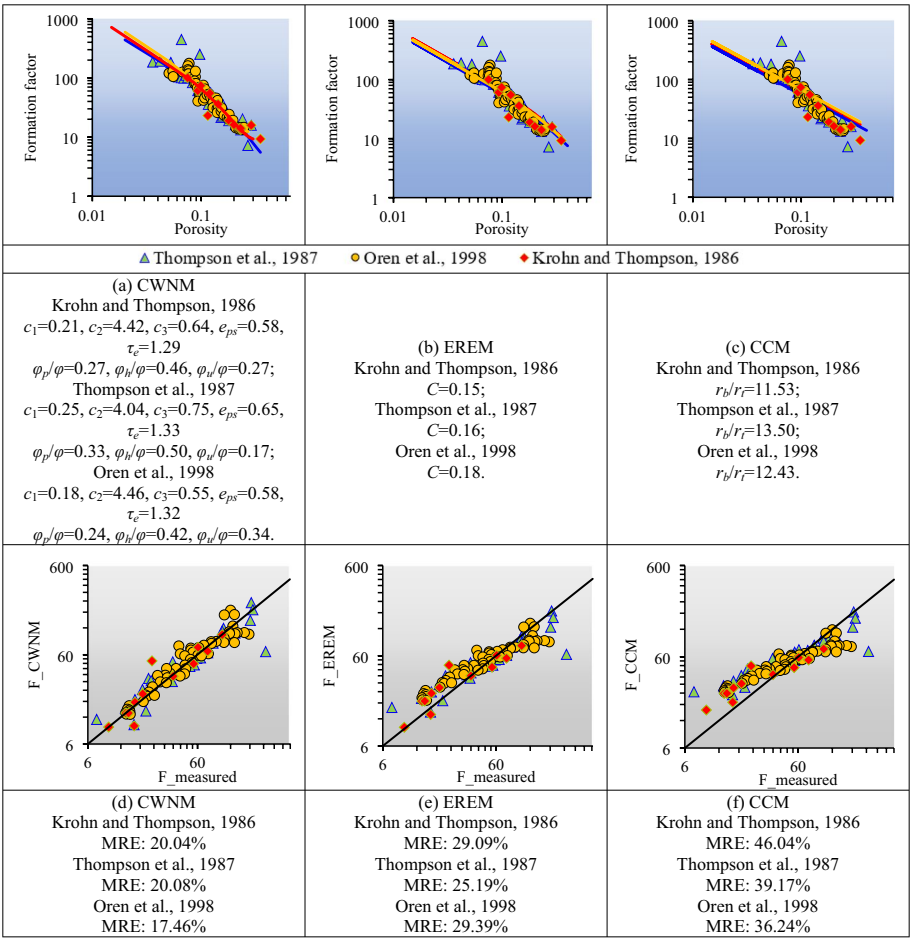

(a) CWNM
Krohn and Thompson, 1986
c_1=0.21, c_2=4.42, c_3=0.64, e_{ps}=0.58, τ_e=1.29
φ_p/φ=0.27, φ_h/φ=0.46, φ_u/φ=0.27;
Thompson et al., 1987
c_1=0.25, c_2=4.04, c_3=0.75, e_{ps}=0.65, τ_e=1.33
φ_p/φ=0.33, φ_h/φ=0.50, φ_u/φ=0.17;
Oren et al., 1998
c_1=0.18, c_2=4.46, c_3=0.55, e_{ps}=0.58, τ_e=1.32
φ_p/φ=0.24, φ_h/φ=0.42, φ_u/φ=0.34.

(b) EREM
Krohn and Thompson, 1986
C=0.15;
Thompson et al., 1987
C=0.16;
Oren et al., 1998
C=0.18.

(c) CCM
Krohn and Thompson, 1986
r_h/r_f=11.53;
Thompson et al., 1987
r_h/r_f=13.50;
Oren et al., 1998
r_h/r_f=12.43.

(d) CWNM
Krohn and Thompson, 1986
MRE: 20.04%
Thompson et al., 1987
MRE: 20.08%
Oren et al., 1998
MRE: 17.46%

(e) EREM
Krohn and Thompson, 1986
MRE: 29.09%
Thompson et al., 1987
MRE: 25.19%
Oren et al., 1998
MRE: 29.39%

(f) CCM
Krohn and Thompson, 1986
MRE: 46.04%
Thompson et al., 1987
MRE: 39.17%
Oren et al., 1998
MRE: 36.24%

Fig. 4 Prediction formation factor effect of CWNM/EREM/CCM on medium–high porosity sandstone. The data points in different colours in **a**–**c** represent the actual rock-electric experiment results. The solid line represents the formation factor–porosity relationship obtained by combining the model parameters obtained from the model with the model; different colours in **a**–**c** represent the formation factor–porosity relationship obtained by the CWNM/EREM/CCM model. The colour of the data points and the line are consistent, which means that they are matched with each other. The obtained formation factor–porosity relationship is obtained by using the matched core data. **d**–**f** Shows the prediction results of the formation factor, where the abscissa is the measured formation factor, and the ordinate is the formation factor predicted by the relationship between the formation factor–porosity provided through (**a**–**c**). The closer they are to the 45° line in the figure, the better the prediction effect. All subsequent similar data graphs use similar visualization methods

from similar strata and locations, the evaluation accuracy can be improved, and inaccurate estimates of the formation factor caused by non-Archie behaviours can be avoided.

Combining the 3 datasets, using the optimization method, the results of the CWNM parameters obtained from different datasets are not identical, but the difference is small, which may be because these three datasets show a similar formation factor–porosity relationship. The EREM/CCM parameters determined by the 3 groups of data are also not

significantly different. Comparing the approximation results of the formation factor and the parameters obtained by the CWNM, EREM, and CCM, the reasons for the differences in model performance can be analysed. The differences between the parameters of the EREM and CCM models for all 3 datasets are quite small, indicating that the determined parameters are reliable and correct.

Figure 4 shows the MRE calculation results for 3 sets of data using 3 models. Taken together, for these 3 sets of data, the average of the 3 MREs determined by the CWNM is 19.19%, the average of the 3 MREs determined by the EREM is 27.89%, and the average of the 3 MREs determined by the CCM is 40.48%. Among them, for the dataset from Thompson et al. (1987), the MRE difference between the CWNM and EREM to obtain the formation factor is the smallest, i.e. 5.11%. When the parameters are obtained for optimization, the data with a larger formation factor are usually approximated first. In this case, some low formation factor data that be affected the accuracy decrease in medium- to high-porosity sandstone for both the EREM and CCM. The effect of the EREM outperforms the CCM in these 3 datasets, suggesting that multiple-pore theoretical models may perform better in medium- to high-porosity sandstone compared to theoretical models when the data suffer from non-Archie behaviours.

An analysis indicates that the CWNM line is significantly more capable of bending downwards (that is, approximating the actual formation factors below the Archie behaviour at low porosity), followed by the EREM and finally the CCM. Relevant studies have shown that the reason for the occurrence of non-Archie behaviours in rock-electric data is the complex pore structure (Hakimov et al. 2019; Sun et al. 2021). CCM has difficulty coping with the non-Archie behaviours of sandstones without considering the differences in the conductivities of different pores in the pore space; this is also what single capillary bundle models not good at. In addition, the calculated results of the formation factor should also confirm the influence of nonconductive pores because the EREM does not consider the existence of nonconductive pores. According to Fig. 4, if the rock-electric data of a conventional medium–high-porosity sandstone exhibit non-Archie behaviours at low porosity and if the lower porosity limit of the reservoir is lower than the low-porosity boundary used to delineate non-Archie phenomena, the CWNM (or at least another multiple-pore theoretical model) should be used. In addition, the appearance of the two formation factor anomalies in the Thompson et al. (1987) data compared with those in similar porosity ranges may be that their pore structures are more complex. Wei et al. (2015) also detected such an anomaly, which was clarified by fractal theory. This also shows that even CWNM, single parameters cannot provide accurate predictions on all rock samples.

5.2 Tight Sandstone

Due to its compaction and the continuous influence of diagenesis, tight sandstone is characterized by a complicated internal pore structure, which further affects the formation factor of the rock. Here, data from 4 papers on 4 different formations: the Shahejie Formation in the Dongpu Depression (Zhang and Weller 2014), the Shihezi Formation in the Sulige area (Li et al. 2017), the Denglouku Formation in the Xiaochengzi area (Zhang et al. 2016b) and the Yanchang Formation in the Ordos Basin (Li et al. 2012), the porosity ranges of these datasets are 7.90–17.40%, 5.99–19.00%, 2.42–16.03% and 5.90–19.00%, respectively, and the corresponding formation factor ranges are 25.40–113.60, 26.60–330.85, 32.57–293.86 and 20.98–88.57. The calculated formation factors from the CWNM, EREM and CCM

are plotted in Fig. 5. First, non-Archie behaviours are still quite obvious, but for tight sandstone, the inflection point that distinguishes non-Archie from Archie behaviours is not evident, and the vast majority of data feature non-Archie behaviour. According to Fig. 5, the average MRE of the CWNM for the 4 sets of tight sandstone data in this section is 13.30%, the corresponding average MRE given by the EREM is 15.18%, and the value given by the CCM is 17.10%. The difference in the MRE between the 3 models is actually very small. In this case, the formation factors calculated by the 3 models essentially match the measured values. The consistency of the data is the main reason why the formation factor calculation accuracy in tight sandstone is higher than that in the conventional sandstone examined above. In this case, the prediction effects of the EREM and the CWNM are similar, suggesting that (in combination with Fig. 4) the CWNM is more suitable when the data exhibit strong complexity, weak consistency, and both Archie and non-Archie behaviours; pure tight sandstones do not require the dedicated use of the CWNM. In addition, when the sandstone rock resistivity data show Archie behaviours, the Archie equation can be used, whereas when completely non-Archie behaviours arise, other multiple-pore theoretical models can be applied.

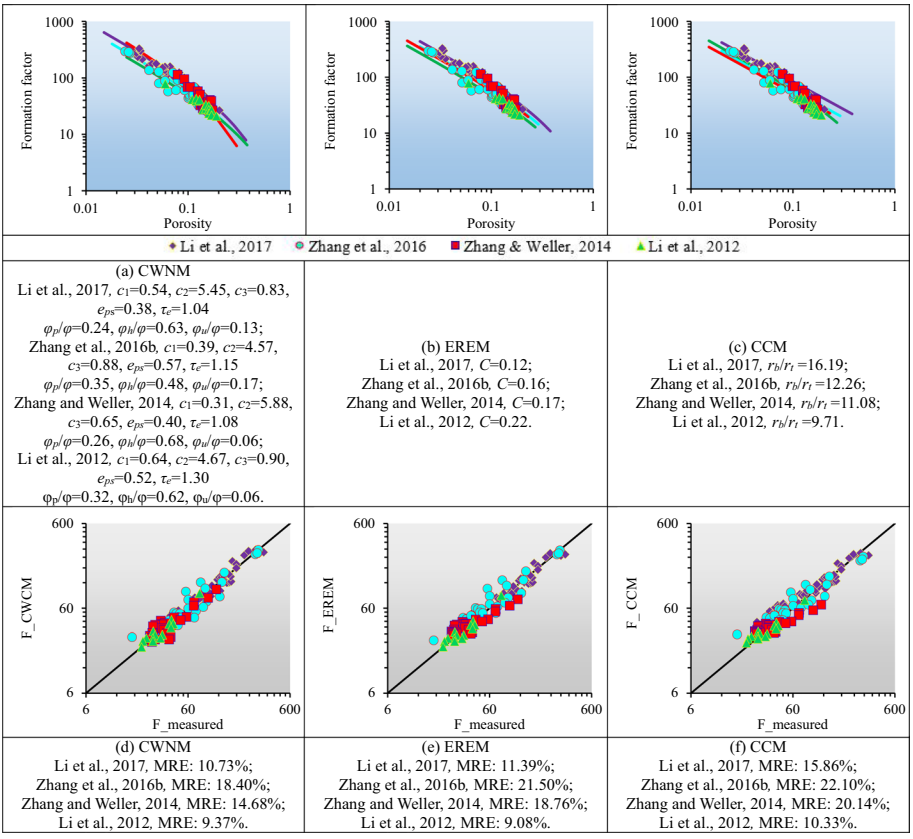

Fig. 5 Prediction formation factor effect of CWNM/EREM/CCM on tight sandstone

Furthermore, comparing the model parameters between Figs. 5 and 4 exposes obvious differences; in fact, even the parameters of different tight sandstones are not identical. For instance, Zhang and Weller (2014) and Li et al. (2017) reported larger c_2 values. Combined with Fig. 5a, these 2 datasets feature similar porosity ranges, and the formation factor is significantly larger than that measured, so the increases in the c_2 values of these 2 datasets are in line with the actual theory. Comparing the results for the conventional sandstone and tight sandstone, their c_1 values differ, and the c_1 of the conventional sandstone is lower than that of the tight sandstone. Considering the previous theoretical analysis, c_1 exerts a main control on the degree of non-Archie behaviours.

5.3 Pore-Dominated Carbonate

Porous carbonate rocks are also characterized by a complex pore structure, although the reason for their complex pore structure is different from that of tight sandstone: there are more intercrystalline pores and dissolved micropores in carbonates, which affect their formation factors. Moreover, the rock-electric data of porous carbonate rocks in different study areas may show various characteristics that do not conform to the Archie equation. Hence, to test the proposed model, data from multiple research blocks are chosen, including data from the Changxing Formation, Yuanba area carbonate, Mishrif and Asmari Formations, Missan area, Mishrif Formation, Halfaya area and eastern Paris Basin limestone (Regnet et al. 2015), among other research data (Nazemi et al. 2019). The pores of the rocks used in these rock resistivity experiments have relatively small fracture contents, so the fairness of the comparison can be ensured. Figure 6 shows the comparison results of the formation factor–porosity relationship between the predictions and core measurements.

Larger formation factor range of porous carbonate rocks is displayed. In general, from the distribution of all rock resistivity data, pore-dominated carbonates obviously have a more complex pore structure and a more diverse relationship between the formation factor and porosity. Except for the data presented by Tang et al. (2017b), in which it is difficult to observe regularity due to the small range of corresponding porosities, the data show strong non-Archie behaviour. From high porosity to low porosity, the slope of the formation factor–porosity curve changes as much as (or even more than) that of either sandstone, which indicates that the pore structure of these carbonate rocks is more complex and diverse.

Figure 6 also shows the MRE results of all 3 models for all datasets. In these datasets, the average MRE for the CWNM is 25.42%, and it achieves the best calculation of the formation factor among all the datasets. The average MRE for the EREM is 32.82%, and the mean for the CCM is 39.14%. In terms of accuracy, for complex pore-dominated carbonate, multiple-pore theoretical models may be superior.

Compared with the CWNM calculation results based on the optimization method, for the units from the Mishrif and Asmari Formations, the Missan area—the Mishrif formation, the Halfaya area and those in Regnet et al. (2015), whose formation factors and porosity ranges are somewhat similar to those of either sandstone, the c_1 values are significantly higher than those of the CWNM, while the e_{ps} values are lower. Their combined ratio of weakly conductive pores to nonconductive pores is also high, which may be an effect of the stronger non-Archie behaviour on the CWNM. The c_2 values determined by these 3 datasets are low; these low values are because the pore sizes of some primary pores in carbonate rocks are enlarged due to dissolution and other effects, while the difference in the pore size between the throats of conductive pores and the pores themselves is reduced (Li et al. 2020; Fheed and Krzyżak 2017). However, the ranges of the optimal parameters

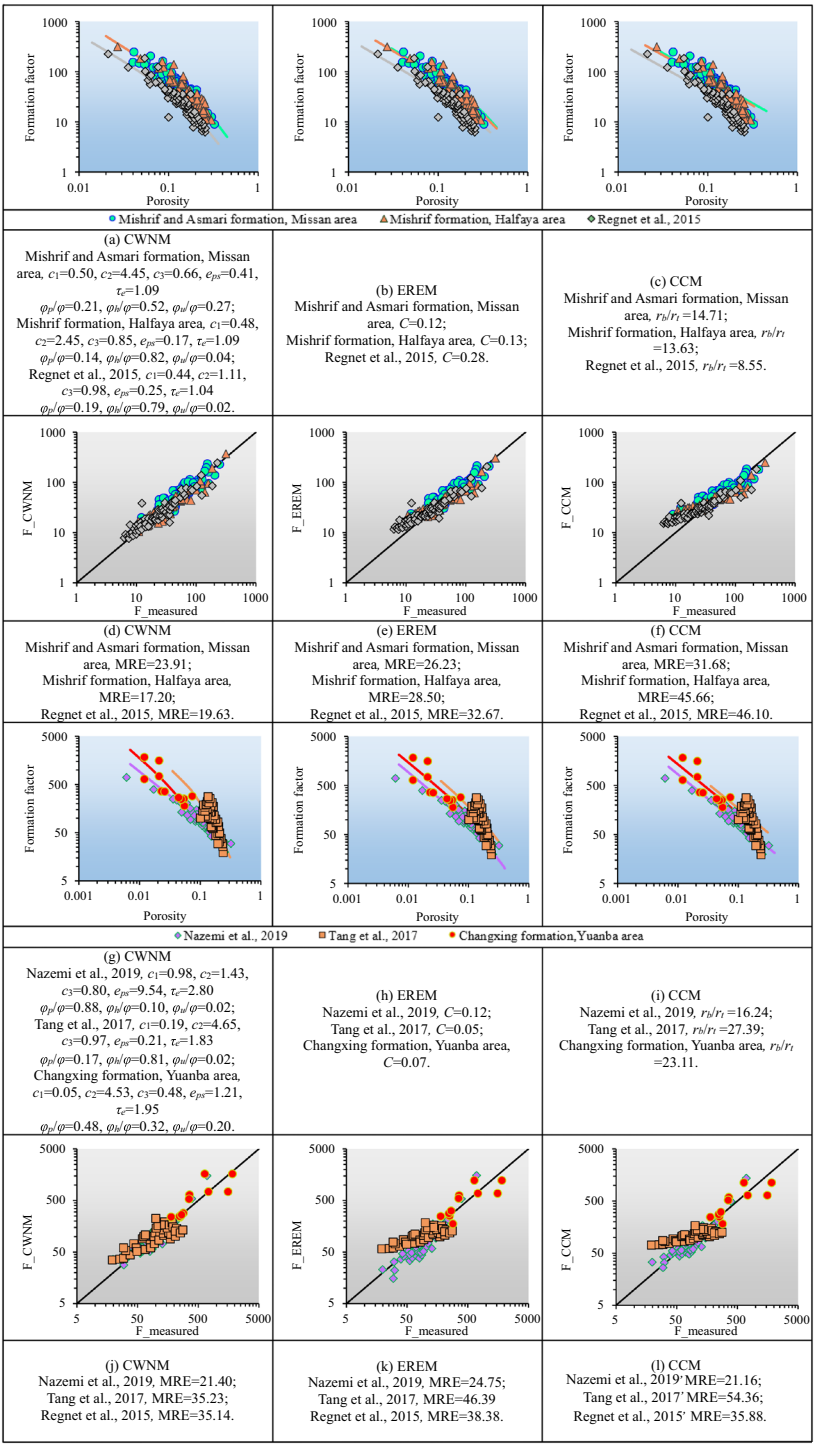

Fig. 6 Prediction formation factor effect of CWNM/EREM/CCM on pore-dominated carbonate

of the EREM and CCM for these three datasets are not greatly different from the sandstone parameters.

In contrast, the formation factor–porosity relationships in Nazemi et al. (2019) and Tang et al. (2017a, b) for the Changxing Formation and the Yuanba area, respectively, are significantly different from those described above. In these cases, the results obtained by combining the parameters of the CWNM model are acutely different from those of other data. For example, for the data of Nazemi et al. (2019), the CWNM parameters are significantly different from those for the data of Li et al. (2017). According to the parameters, the nonconductive porosity is low, the proportion of conductive and weakly conductive pores is high, and the electrical tortuosity is high. In brief, the CWNM can be used for pore-dominated carbonates.

5.4 Shale

The formation factor calculation effect of the CWNM should also be investigated for more complex reservoir rocks, such as shales (Cai et al. 2018; Song and Kausik 2019; Foroozesh et al. 2019; Li et al. 2022). The electrical conductivity of shale is influenced by its complex pore structure, wettability, and fluid distribution, as well as by its diverse composition of conductive minerals (Zhu et al. 2021, 2022). The thermal evolution of shale also affects the organic pore system and the inorganic pore system, resulting in changes in pore structure characteristics (Gao et al. 2020). All these factors affect the formation factor. Here, data from shale reservoirs in China and Australia are selected to test our model (Fan et al. 2018; Malekimostaghim et al. 2019; Zhong et al. 2021, 2022). However, it is difficult to carry out petrophysical experiments on shale because it is fragile; therefore, the available shale petrophysical test data are sparse. The shale data from Australia are derived from publicly published literature, while the rock-electric data from the Longmaxi Formation shale in Sichuan, China, are derived from data collected in the present study. Studies have shown that when the water resistivity in the pores of shale rock is lower than approximately 0.1 Ω. m, the surface conductivity can be ignored (Zhong et al. 2022). However, the corresponding water resistivity of the data set selected in this paper is much lower than 0.1 Ω. m. These shale datasets are quite different from each other, with porosities ranging from 0.017 to 0.205 and formation factors ranging from 14.38 to 7510, indicating that shales produced in different locations vary far more than either sandstones or carbonates. It should be noted that the contents of conductive minerals, such as pyrite and haematite, in these rock samples are quite small, not exceeding 3%, and all data exceeding this limit are excluded. In addition, the literature from which the data were derived verified that the surface conductivity and cation exchange capacity of these data are not sufficient to have a remarkable influence on the rock's resistivity; thus, the overall resistivity was analysed by using these data. For some data, high-salinity brines were used to limit the strong cation exchange capacity.

Figure 7 shows all the formation factors derived from the shale resistivity data. From the resistivity data alone, the differences between the two shales seem substantial, much larger than those among the sandstones. This difference may occur because shales span a wider variety of compositions. Moreover, in basically all of the shale data, the formation factor is large, which reflects the complex pore structure of shale. However, according to the parameters obtained by the CWNM, although data from different sources have large formation factors, their conductivity characteristics are different. For instance, the Longmaxi Formation and Yongchuan area data have relatively high e_{ps} and c_3 values, indicating that

the proportion of conductive pores and weakly conductive pores is considerable. According to the calculation of Eq. (49) in Appendix 3, the proportion of conductive pores is 48.54%, and the proportion of weakly conductive pores is 49.92%. In comparison, the data of Zhong et al. (2021) yield abnormally low e_{ps} values and high c_3 values, which indicates that this dataset has a high proportion of pores that have difficulty conducting electricity (the proportion of weakly conductive pores computed by Eq. (49) is 71.41%). The data of Zhong et al. (2022) also yield a higher calculated proportion of nonconductive pores (62.92%) because c_1 is relatively high and c_3 is relatively low.

Figure 7 also shows the MRE of the three models for the four sets of data. The average MRE of the CWNM is 26.32%, and the average MRE values of the EREM and CCM are 29.32% and 32.40%, respectively. We cannot definitively state whether the differences in the accuracy of different models are entirely due to differences in the assumptions of the models because the sample size is indeed insufficient. It should be said that for shale, according to the current results, the differences in the effects of such theoretical models are not obvious.

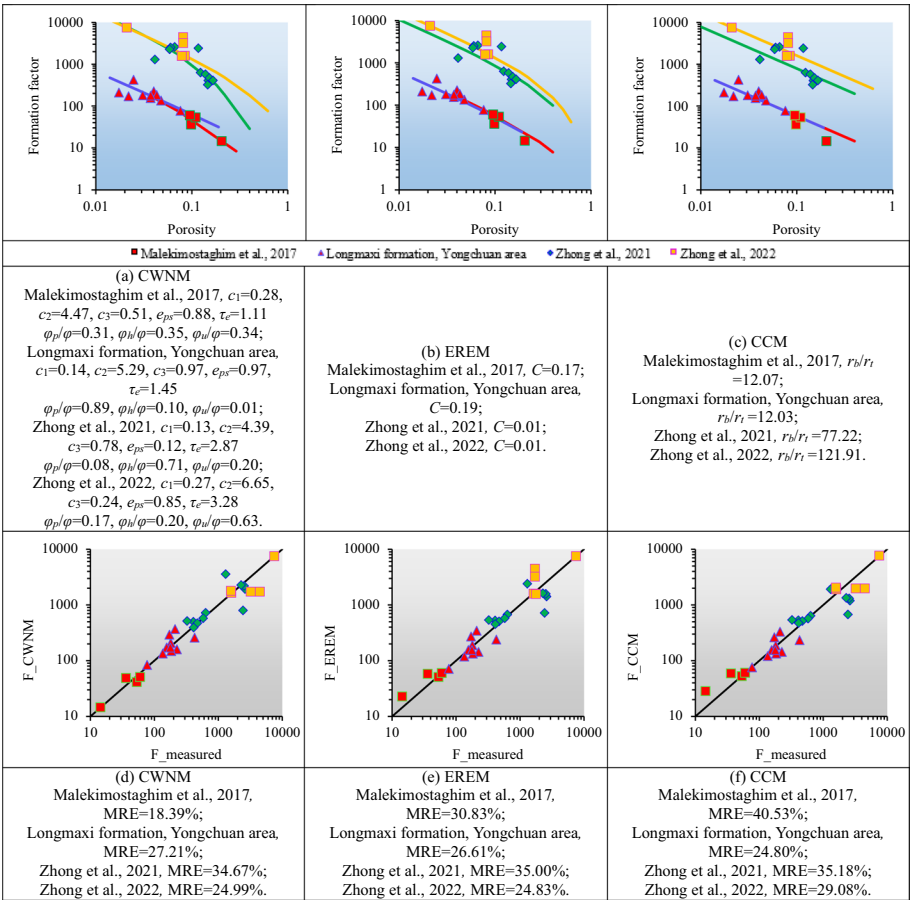

Fig. 7 Prediction formation factor effect of CWNM/EREM/CCM on shale

Based on the parameter results of the CWNM/EREM/CCM, the model parameters of the EREM and CCM are undoubtedly easier to determine. In the case of sufficient rock resistivity data of shale, CWNM is a better choice, but if the amount of data is small, it is EREM and other multiple-pore theoretical models with fewer parameters. Their parameters may be easier to determine.

5.5 Andesite

Andesites can also serve as reservoirs with a complex pore structure (Guo et al. 2022). For instance, a large number of andesite reservoirs have been discovered in China's Bohai Bay Basin and Sichuan Basin, showing the potential of such reservoirs. Thus, to analyse our model, the rock-electric data summarized in Li et al. (2014) are used, whose results are shown in Fig. 8.

From a data point of view, the formation factors presented by this group of rock resistivity data exhibit a large rate of change with varying porosity. This feature is somewhat similar to the data from the Changxing Formation and Yuanba area. Figure 8 shows the difference in the accuracies of the three models. In this dataset, the MRE given by the CWNM is much lower than that of the other models. Andesite is generally prone to developing fractures with high aspect ratios; this occurrence may indicate that the CWNM has a certain applicability in fractured reservoirs, which requires follow-up targeted research for confirmation. According to the predicted formation factors, andesites contain weakly conductive pores and nonconductive pores, and their impact needs to be considered. It is worth noting that the MRE of CWNM for the Li et al. (2014) data set is 26.95%, which is about 96.5% lower than the predicted MRE from CCM.

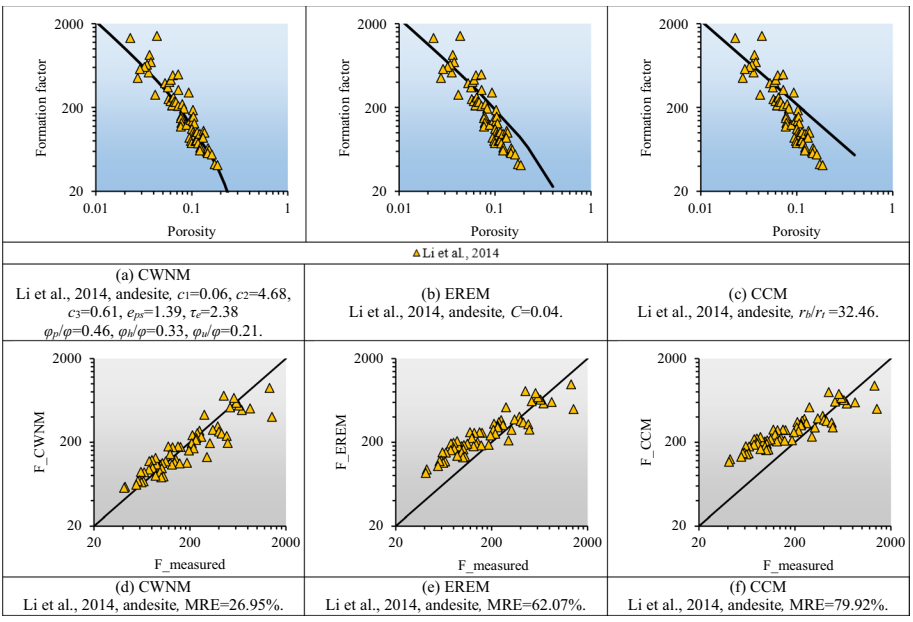

Fig. 8 Prediction formation factor effect of CWNM/EREM/CCM on andesite

5.6 Permafrost and Marine Gas Hydrate Reservoir Rocks/Sediments

Natural gas hydrates are an emerging source of fossil energy that have been discovered mainly in permafrost regions on land and in marine environments. In the deep sea, gas hydrates are stored in extremely high-porosity sediments, which are usually in the early stages of diagenesis and are not consolidated, whereas the gas hydrates in permafrost regions are present in subsurface rocks. This paper selects rock-electric data from permafrost in the Qilian Mountains (Guo 2011; Dong et al. 2020) and the marine Ulleung Basin (Riedel et al. 2013) to compare different models and explore their applicability.

Figure 9 clearly shows that the characteristics of the data from the permafrost region and the marine gas hydrate reservoir rocks/sediments are considerably different, which is slightly similar to the comparison of resistivity data between carbonate rocks and shale. The formation factor–porosity relationship features strong non-Archie behaviours, such as in the data from Dong et al. (2019). From the perspective of the CWNM parameters, the c_1 and e_{ps} parameters are relatively small, and the proportion of weakly conductive pores is quite large. These results may be characteristic of permafrost gas hydrate reservoir rocks. In a similar porosity range, the formation factor of Dong et al. (2019) is larger. Considering all the parameters, Dong et al. (2019) predicted fewer conductive pores, and the c_2 of the conductive pores is higher (higher than the c_2 obtained from the sandstone and tight sandstone data).

Figure 9 also shows the prediction accuracy of the formation factor with 3 models for 5 datasets. For the provided permafrost gas hydrate reservoir rock dataset, the average MRE results of the two datasets predicted by the CWNM are 35.44%, while the average MRE results of the EREM and CCM are 85.72% and 112.01%, respectively. For the above two permafrost gas hydrate reservoir rock datasets, multiple-pore theoretical models may be better. The CWNM performs better than the EREM for the above datasets, especially for the dataset shown by Guo (2011). In the dataset given by Guo (2011), some of the data have produced obvious non-Archie behaviours, which may be the reason for the effectiveness of the CWNM. These data are somewhat similar to those of the conventional medium- to high-porosity sandstone. Looking at the prediction performance of the three datasets of marine gas hydrate reservoir sediments, the average MRE of the three CWNM datasets is 6.11%, while the average MRE values of the three EREM and CCM datasets are 13.44% and 17.07%, respectively. Moreover, all the CWNM datasets of marine gas hydrate reservoir sediments are stable. In conclusion, the electrical conductivity of gas hydrates reservoirs can be analysed by combining the parameters of the CWNM.

5.7 Rock-Electric Data with Extreme Features that Do not Follow the Archie Equation Behaviours

In addition, we further explore new model's ability to approximate rock-electric data that are extremely inconsistent with the behaviours stipulated by the Archie equation. Zhang (2020) reported the rock-electric data of an oil area in Kazakhstan involving a sandstone reservoir with highly complex conductivity characteristics, and all data were derived from the same set of formations. The data showed an important example of non-Archie behaviours; consequently, Zhang (2020) could determine the calculation equation for the formation factor only by piecewise fitting, using the porosity value as the boundary. However, theoretically, even if there are differences between different rock samples, these differences

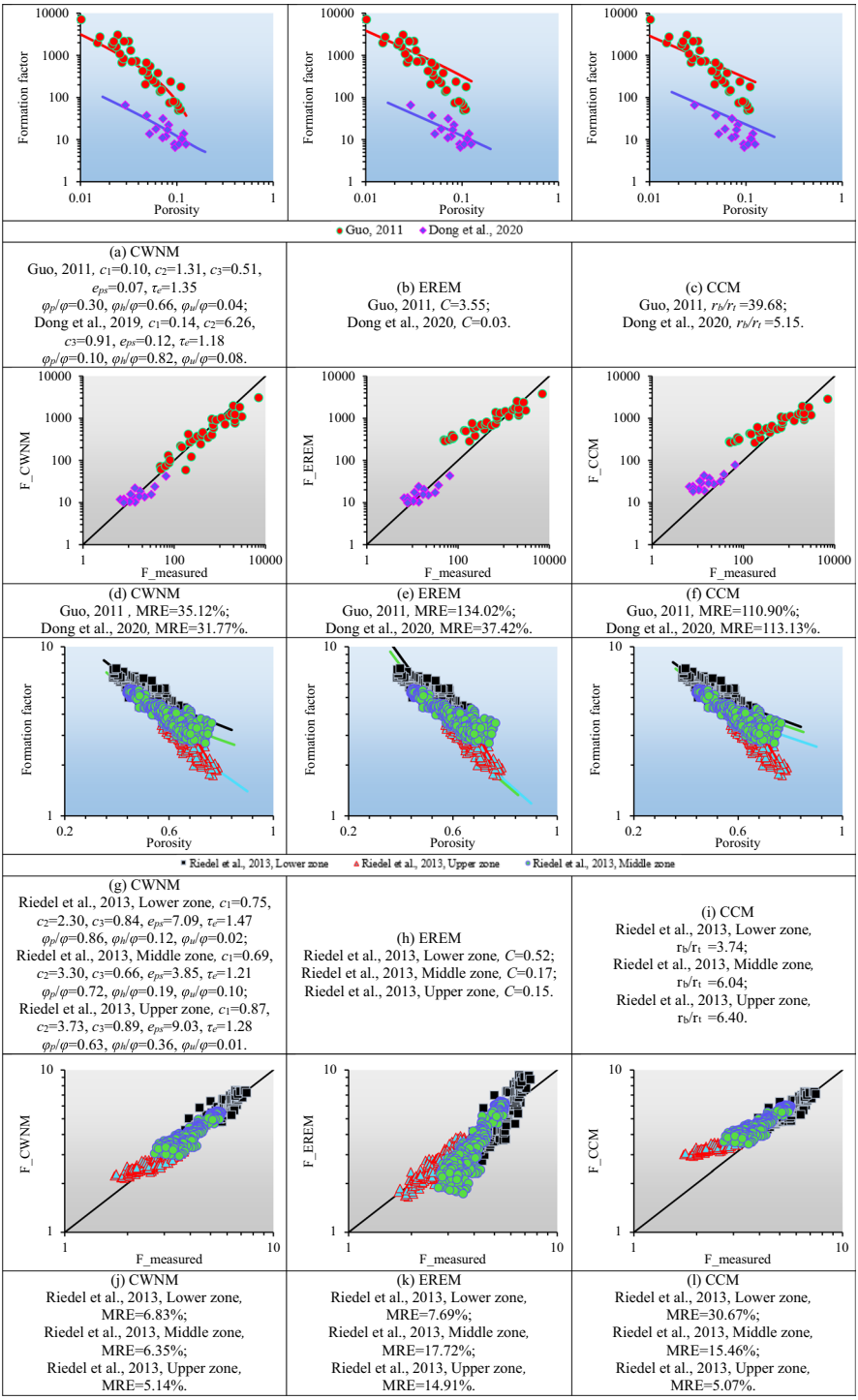

(a) CWNM
Guo, 2011, c_1=0.10, c_2=1.31, c_3=0.51, e_{ps}=0.07, τ_e=1.35
φ_p/φ=0.30, φ_h/φ=0.66, φ_u/φ=0.04;
Dong et al., 2019, c_1=0.14, c_2=6.26, c_3=0.91, e_{ps}=0.12, τ_e=1.18
φ_p/φ=0.10, φ_h/φ=0.82, φ_u/φ=0.08.

(b) EREM
Guo, 2011, C=3.55;
Dong et al., 2020, C=0.03.

(c) CCM
Guo, 2011, r_b/r_t =39.68;
Dong et al., 2020, r_b/r_t =5.15.

(d) CWNM
Guo, 2011 , MRE=35.12%;
Dong et al., 2020, MRE=31.77%.

(e) EREM
Guo, 2011, MRE=134.02%;
Dong et al., 2020, MRE=37.42%.

(f) CCM
Guo, 2011, MRE=110.90%;
Dong et al., 2020, MRE=113.13%.

(g) CWNM
Riedel et al., 2013, Lower zone, c_1=0.75, c_2=2.30, c_3=0.84, e_{ps}=7.09, τ_e=1.47
φ_p/φ=0.86, φ_h/φ=0.12, φ_u/φ=0.02;
Riedel et al., 2013, Middle zone, c_1=0.69, c_2=3.30, c_3=0.66, e_{ps}=3.85, τ_e=1.21
φ_p/φ=0.72, φ_h/φ=0.19, φ_u/φ=0.10;
Riedel et al., 2013, Upper zone, c_1=0.87, c_2=3.73, c_3=0.89, e_{ps}=9.03, τ_e=1.28
φ_p/φ=0.63, φ_h/φ=0.36, φ_u/φ=0.01.

(h) EREM
Riedel et al., 2013, Lower zone, C=0.52;
Riedel et al., 2013, Middle zone, C=0.17;
Riedel et al., 2013, Upper zone, C=0.15.

(i) CCM
Riedel et al., 2013, Lower zone, r_b/r_t =3.74;
Riedel et al., 2013, Middle zone, r_b/r_t =6.04;
Riedel et al., 2013, Upper zone, r_b/r_t =6.40.

(j) CWNM
Riedel et al., 2013, Lower zone, MRE=6.83%;
Riedel et al., 2013, Middle zone, MRE=6.35%;
Riedel et al., 2013, Upper zone, MRE=5.14%.

(k) EREM
Riedel et al., 2013, Lower zone, MRE=7.69%;
Riedel et al., 2013, Middle zone, MRE=17.72%;
Riedel et al., 2013, Upper zone, MRE=14.91%.

(l) CCM
Riedel et al., 2013, Lower zone, MRE=30.67%;
Riedel et al., 2013, Middle zone, MRE=15.46%;
Riedel et al., 2013, Upper zone, MRE=5.07%.

Fig. 9 Prediction formation factor effect of CWNM/EREM/CCM on permafrost and marine gas hydrate reservoir rocks/sediments

should not be directly related to porosity. Here, the proposed model to approximate these data is attempted to apply. To facilitate a comprehensive comparison, the fitting effects of 8 other models are also shown, including the following 3 models in addition to the models introduced above:

$$\text{Herrick and Kennedy (2009)}: \quad F = \frac{1}{E_o \varphi} \tag{33}$$

$$\text{Ghanbarian and Berg (2017)}: \quad F = \begin{cases} \frac{(1-\varphi_c)(\varphi_x-\varphi_c)}{(\varphi-\varphi_c)^2}, & \varphi_c < \varphi < \varphi_x \\ \frac{1-\varphi_c}{\varphi-\varphi_c}, & \varphi_x < \varphi < 1 \end{cases} \tag{34}$$

Song et al. (2014):

$$F = \frac{\lambda_{ma}\left((1-\varphi)^{\gamma_1} + \varphi_{wne}^{\gamma_1}\right)\left(1-\varphi+\varphi_{wne}\right) + \lambda_w\left(\varphi-\varphi_{wne}\right)^{\gamma_2}\left(3-\left(\varphi-\varphi_{wne}\right)\right)}{2\lambda_w\left(\varphi-\varphi_{wne}\right)^{(\gamma_2+1)}} \tag{35}$$

In Eqs. (33)–(35), E_o refers to the geometrical factor; φ_c refers to the critical porosity; φ_x refers to the crossover porosity; φ_{wne} refers to the ineffective conductive porosity; λ_w refers to the percolation rate; γ_1 refers to the ineffective conductive pore percolation coefficient; and γ_2 refers to the pore percolation coefficient.

Figure 10 shows the prediction results of a total of 8 methods for these characteristic data. Overall, the multiple-pore theoretical models achieved better results. The MREs of the CWNM, EREM, method proposed by Song et al. (2014), method proposed by Li et al. (2017) and method proposed by Meng and Liu (2019) were 19.40%, 39.57%, 32.52%, 34.92% and 41.32%, respectively. These results should support the previously stated theory that multiple-pore theoretical models are more suitable for non-Archie behaviour data. The CWNM also performs well and is the only model with an MRE less than 20% for the data in this section. Others, such as the method proposed by Ghanbarian and Berg (2017) based on percolation theory, may not be well suited to such data with strong non-Archie behaviours.

In addition, a larger number of parameters do not necessarily correspond to a stronger approximation ability. For example, the PTM and Meng and Liu model are not as effective as the EREM in these data, but they have more parameters. The assumptions that are closer to the conductivity features are the most important. Figure 10 presents a further comparison of the effects of each model on the selection of lithological data.

5.8 Comparison of Model Parameters and Accuracy of the CWNM in Different Lithologies

The CWNM has many model parameters, causing it to exhibit great flexibility. This flexibility guarantees the prediction effect of the model for the formation factor. After Sects. 5.1, 5.2, 5.3, 5.4, 5.5, 5.6 and 5.7, based on data, the parametric laws of lithology with different characteristics can be analysed, as well as the MRE results, and the summary table is shown in Figs. 4, 5, 6, 7, 8, 9 and 10. It shows that for the performance of the CWNM, the performance of the CWNM in sediments and various types of sandstone is more stable, while the performance in pore-dominated carbonate and shale is relatively

weak. The MRE can basically be maintained at less than 35%. Among the 24 datasets, 19 datasets have MRE values less than 30%, accounting for 79.17%. In addition, CWNM can reduce the relative error rate by 96.5% compared to other models used for comparison, a result that appears in the andesite lithology.

The differences in the CWNM model parameters of sandstone, carbonate rock, shale, andesite, hydrate reservoir rock in permafrost, marine hydrate reservoir sediment, etc. can be compared (Figs. 4, 5, 6, 7, 8, 9 and 10). In combination with the previous theoretical analysis, c_1 controls the change in the slope of the formation factor–porosity relationship. When c_1 is small, the change in the slope under the double logarithmic coordinate axis is more obvious with the change in porosity. However, data with non-Archie behaviours generally exhibit a reduced slope of the formation factor–porosity relationship at lower porosity data locations. Therefore, to accurately predict the formation factor with data with non-Archie behaviours, the value of c_1 should be low. Based on the prediction results, if only sandy rocks or sediments are analysed (including conventional medium- to high-porosity sandstone, tight sandstone, permafrost and marine gas hydrate reservoir rocks/sediments,

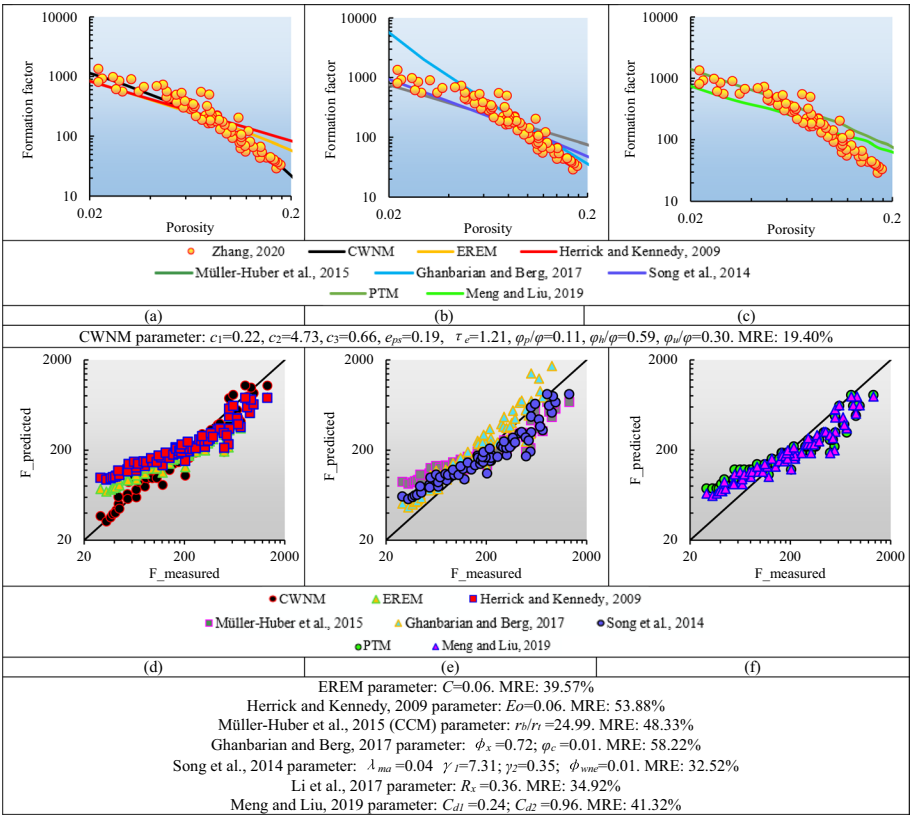

Fig. 10 Effect of 8 formation factor calculation models on rock-electric data with extreme features that do not conform to the Archie equation. The 8 lines of different colours represent the prediction results of the data points using the 8 formation factor calculation models. Only the CWNM can accurately predict the formation factor in the entire porosity range of 0.2–20%, and other models can only be used to predict the formation factor in the partial porosity range

and rock-electric data with extreme features that do not follow the Archie equation behaviours), for some data with non-Archie behaviours and some data with strong non-Archie behaviour, the c_1 value is lower, and the statistical mean is 0.19. Furthermore, the value of c_1 combined with data with fully non-Archie behaviour is also stable and not very low, as the data in such datasets have relatively low porosity, and the inflection point that distinguishes non-Archie from Archie behaviours is not evident; the data pattern is more consistent. In this case, the mean c_1 is 0.47. This indicates that c_1 is a key parameter of the CWNM. In terms of lithology, the datasets of conventional medium- to high-porosity sandstone, shale, andesite and permafrost gas hydrate reservoir rocks all show low c_1 values, while the datasets of tight sandstone show moderate c_1 values. The datasets of marine gas hydrate reservoir sediments show a high c_1 value, while the parameters of different datasets of pore-dominated carbonate are very different, which may be due to the complex pore structure caused by multiple factors. Among them, the dataset parameters of some data with non-Archie behaviour in pore-dominated carbonate are relatively stable, showing a moderate c_1 value. This result illustrates the difference in conductivity characteristics between pore-dominated carbonate and sandstone-like reservoirs.

The larger c_2 is, the more heterogeneous the conductive pores are; in addition, the formation factor increases, and a positive correlation is present between them. Based on the parameter results, the c_2 values of conventional medium- to high-porosity sandstone range from 4 to 4.5, while those of tight sandstone are greater than 4.5, which reflects the differences between different sandstones. The c_2 values of the data based on pore-dominated carbonate are basically less than 4.5, which is different from the characteristics of the above two sandstones. The complex pore structure of pore-dominated carbonate is due to the complex pore types, while sandstone and tight sandstone have complex pore structures due to the complex pore throat relationship. Since the pore sizes of secondary pores and primary pores are often different, the pore heterogeneity of a single pore type is not strong, and the c_2 value of pore-dominated carbonate is lower than that of sandstone. Shale has complex pore throat relationships and diverse pore structures, with a c_2 value of up to 6.65. The c_2 of marine gas hydrate reservoir sediments is the smallest because of its simpler pore structure and lower pore heterogeneity than those of tight rocks.

c_3 reflects the proportion of weakly conductive pores in the total of weakly conductive pores and nonconductive pores. The previous parameter simulation shows that the smaller the value of c_3 is, the larger the formation factor. As compaction and diagenesis are continuously enhanced, some conductive pores gradually evolve into weakly conductive pores, and weakly conductive pores gradually change to nonconductive pores. Therefore, with the densification of pores, the change in c_3 is not necessarily monotonic. The conventional medium- to high-porosity sandstone has an average c_3 value of 0.65, rock-electric data with extreme features that do not follow the Archie equation behaviours have an average c_3 value of 0.66, and the tight sandstone has an average c_3 value of 0.82. In addition, the c_3 values of different rocks or sediments are basically greater than 0.5, which indicates that weakly conductive pores have usually higher porosity than nonconductive pores in actual rocks or sediments. For the shale data, the data given by Zhong et al. (2022) do not conform to this rule. By observation, in this dataset, in 8.5% of the porosity data, the corresponding formation factor can reach 1500, and it is normal for the content of nonconductive pores to be high. Combined with Fig. 7, the proportion of nonconductive pores in this dataset reaches more than 60%.

The e_{ps} reflects the volume ratio of conductive pores to weakly conductive pores, and the smaller the value is, the larger the formation factor. Based on the patterns reflected by different lithologies, in addition to the strong parameter stability of different datasets of

conventional medium- to high-porosity sandstone, tight sandstone and marine gas hydrate reservoir sediments, the differences in e_{ps} parameters between different datasets of other lithologies are larger. Combined with Figs. 4, 5, 6, 7, 8, 9 and 10, datasets with large differences in parameters are usually due to differences in the formation factor and porosity distribution of the data. For example, compared with other pore-dominated carbonates, Nazemi et al. (2019) show a high e_{ps}, which is reasonable considering the prediction results. According to the results given in the dataset, when the porosity is 1%, the formation factor of the data should be only approximately 600, which is a very low formation factor compared to that of other datasets. The calculation shows that the proportion of conductive pores is as high as 0.88. These results indicate that e_{ps} is a parameter that macroscopically controls the range of the distribution of formation factor values.

τ_e is a common parameter that characterizes the electrical conductivity of porous media. The range of τ_e values for different datasets in sand-like porous media, such as conventional medium- to high-porosity sandstone, tight sandstone, permafrost and marine gas hydrate reservoir rocks/sediments, as well as rock-electric data with extreme features that do not follow the Archie equation behaviours, is stable. The range of τ_e values for rock types such as pore-dominated carbonate and shale is different in different datasets, and these lithologies have the characteristics of diverse pore types. The tortuosity of different pore types developed in the pores is different, which may be the reason for the difference in their own tortuosity. The rule of τ_e is relatively simple, and the related research is also very thorough.

6 Discussion

The characterization of the electrical properties of complex porous media has always been a focus of many scholars because it is the key basis for geophysical methods (electromagnetic and resistivity logging) using electricity as a means. This paper presents a novel multiple-pore theoretical model for characterizing the single-phase conducting behaviour of complex porous media, which is called the CWNM. Our new view is that the entire pore space should be divided into nonconductive pores, weakly conductive pores and conductive pores. This distinction is first proposed based on the effect of pore structure on the electrical conductivity of the pore space. It contains 5 parameters, namely c_1, c_2, c_3, e_{ps}, τ_e, which refer to the ratio of the sum of the cross-sectional areas of weakly conductive pores and nonconductive pores to the cross-sectional area of the entire rock, the pore scaling factor, the ratio of the cross-sectional area of weakly conductive pores to the sum of the cross-sectional areas of weakly conductive pores and nonconductive pores, the volume ratio of conductive pores to weakly conductive pores and the tortuous conductivity of the pore space, respectively. The role played by the same parameters is not exactly the same, and the model has strong flexibility. Combined with optimization algorithms, such as genetic algorithms, the effective values of these five parameters can help the CWNM predict a reliable formation factor. The formation factors are predicted in 24 datasets derived from various lithologies, and good results are obtained. This paper finds that it is feasible to divide pores and establish models according to the conductive characteristics of pores. This gives a high-precision model, but also, more importantly, provides a new research idea for establishing conductivity models for scholars who are engaged in related research in the future.

The corresponding numerical simulation or experimental research is not current. Some areas in the model still need to be further researched. First, the CWNM parameters are currently calculated via optimization method. Thus, how to calculate the CWNM parameters

according to actual rock samples needs to be explored. Our follow-up plan is to carry out numerical simulations on electrical conductivity data based on digital rock physics. Both the formation factor and the porosity can be easily determined by combining finite element simulations with digital rocks (Andrä et al. 2013; Nie et al. 2016; Zhu et al. 2019; Saxena et al. 2021; Sawayama et al. 2021a, 2021b; Li et al. 2022). Then, according to the electrostatic field amplitudes of the entire pore space, the pore space can be classified, the proportions of different types of pores can be determined, and c_3 and e_{ps} can be ascertained. The pore radii of conductive pores and c_2 can be calculated, as can τ_e based on digital cores, as this technique is quite mature. Finally, the remaining parameter (c_1) can be calculated. In recent years, some parameters of formation factor models have been obtained by following this approach.

Second, a complete set of methods to evaluate the CWNM parameters based on actual rock microscopic pore structure parameters has not yet been established, but such evaluations are the key to calculating reservoir formation factors based on geophysical data, such as well logging. Numerical simulation studies are also needed to determine the relationship between CWNM parameters and pore structure parameters for different types of reservoirs. In the best case, five CWNM parameters can be determined by fewer than five pore structure parameters, which makes our model more practical.

Finally, the development of the above theory should be applied not only to calculate the formation factor but also to evaluate the degree of saturation, which aids in the exploration and development of oil and gas and hydrate reservoirs, as well as practical engineering tasks, such as CO_2 sequestration and H_2 geological storage. Consequently, future research will also focus on this theme.

7 Conclusions

In this work, the focus is on finding a method to more accurately characterize the formation factors of various pore-dominated reservoirs. Using the truncated cone pores as the basis in combination with the actual pore conductive characteristics of conductive pores, weakly conductive pores and nonconductive pores to describe the conductivity characteristics of the entire pore space, a new method, the CWNM, was developed to calculate the formation factor. The tortuous conductivity τ_e and the related parameters, namely c_1, c_2, c_3 and e_{ps}, which are used to characterize conductive pores, weakly conductive pores and nonconductive pores, jointly determine the formation factor–porosity relationship; they each represent the tortuous conductivity of the pore space, ratio of the sum of the cross-sectional areas of weakly conductive pores and nonconductive pores to the cross-sectional area of the entire rock, area ratio of the pore with the widest cross-sectional area to the pore with the narrowest cross-sectional area among the truncated cone pores, cross-sectional area of weakly conductive pores to the sum of the cross-sectional areas of weakly conductive pores and nonconductive pores, and volume ratio of conductive pores to weakly conductive pores, respectively. In the CWNM, c_1, c_2 and τ_e show a significant positive correlation with the water-saturated rock resistivity, whereas c_3 and e_{ps} show a negative correlation with resistivity; they determine the relationship between the formation factor and φ. Compared with the existing models, the proposed model provides a more general assumption and a more general model form. The proposed model can be applied to various types of rocks, including conventional medium- and high-porosity sandstones, tight sandstones, porous carbonate rocks, shales, andesites, permafrost and marine gas hydrate reservoir rocks/sediments, and rock-electric data that fail to conform to the Archie equation. A total of 24 sets

of rock-electric data were calculated based on the proposed model's parameters, and the prediction accuracy of the CWNM was compared with that of other models. The CWNM achieved the most accurate results for almost all lithologies, which reflects the extraordinary effect of the proposed model. In evaluating the performance of the formation factor on the dataset used in the paper, CWNM can reduce the relative error by up to 96.5%. Moreover, our model can clarify the pore space electrical conductivity characteristics of different types of reservoirs from the obtained parameters. Ultimately, when the slope of the formation factor–porosity relationship of a certain reservoir varies widely or the slope cannot be characterized by an existing model, adopting the CWNM is strongly recommended. Future research on the CWNM should focus on parameter determination, parameter evaluation and saturation evaluation applications. This work shows that it is appropriate to assume that the entire pore space comprises pores with three levels of conductivity, even marine gas hydrate reservoirs with very high porosity have many weakly conductive pores.

Appendix 1: Derivation of Eq. (4)

In Appendix 1, combined with Fig. 1, the radius of the smaller end of the cross-sectional area of the pore is $r_{\min}$, and the radius of the larger end of the cross-sectional area of the pore is $r_{\max}$. According to this assumption, the resistance r_g of the conductive pores is calculated, and the equation is as follows:

$$r_g = \int_0^{L_g} R_w \frac{dl}{S(l)} = \frac{1}{\pi r(l)^2} dl \tag{36}$$

Among them, $r(l)$ refers to the values of the radius of the circle where the pore length is l, $0 \le l \le L_g$. Here, for the convenience of derivation, the cross-sectional area of the pores varies is set uniformly; then:

$$r_g = \frac{1}{\pi} \int_0^{L_g} \frac{1}{\left[r_{\min} + \left(r_{\max} - r_{\min}\right)\frac{l}{L_g}\right]^2} dl \tag{37}$$

Equation (37) must determine the relationship between $r_{\max}$ and $r_{\min}$ for further equation transformation. To facilitate the calculation of the subsequent parameters, the parameter c_2 to characterize their differences is introduced. We do not introduce the two parameters to characterize the subsequent model application, and the parameters should be as few as possible. Thus:

$$r_{\max} = c_2 r_{\min} \tag{38}$$

Combining Eqs. (37) and (38), the equation changes to the following:

$$r_g = \frac{R_w}{\pi} \int_0^{L_g} \frac{1}{\left[r_{\min} + \left(c_2 - 1\right) r_{\min}\frac{l}{L_g}\right]^2} dl \tag{39}$$

Solving this equation, the resistivity of a single conductive pore can be finally obtained, namely Eq. (40):

$$r_g = \frac{R_w L_g^2}{\pi r_{\min}^2 (c_2 - 1)\left[L_g + (C_2 - 1)l\right]}\Big|_{l=0}^{l=L_g} = \frac{R_w L_g}{\pi c_2 r_{\min}^2} \tag{40}$$

Appendix 2: Derivation of Eq. (15)

Equations (14) and (15) in the main text skip the derivation of multiple assumptions and simple steps and are specifically elaborated in Appendix 2. Assuming that $\overline{S}$ is the average cross-sectional area of the rock occupied by a single conductive pore (truncated cone pore):

$$\overline{S} = \frac{S}{\sum_{i=1}^{O} F_i} = \frac{\pi \overline{r_m}^2 L_1}{\varphi_p L} = \frac{\pi \overline{r_m}^2 \tau_e}{\varphi_p (1+e)} \tag{41}$$

where φ_p refers to the porosity of all conductive pores (or truncated cone pores). Substitute Eq. (41) into Eq. (14), where the number of pores with pore scaling factor c_{2i} and the minimum radius is $\mathrm{r}_{\mathrm{min}i}$ in the total number of conductive pores is f_{i}:

$$F = \frac{\tau_e \overline{S}}{\pi(1+e)}\left(\frac{\sum_{i=1}^{O} F_i c_{2i} r_{\min i}^2}{\sum_{i=1}^{O} F_i}\right)^{-1} + \frac{e\tau_e}{(1+e)c_1 c_3} = \frac{\tau_e^2}{(1+e)^2}\frac{\overline{r_m}^2}{\varphi_p}\left(\sum_{i=1}^{O} f_i c_{2i} r_{\min i}^2\right)^{-1} + \frac{e\tau_e}{(1+e)c_1 c_3} \tag{42}$$

After obtaining Eq. (42), the P_i parameter is defined. The P_i parameter refers to the ratio of the average radius values to the minimum radius of the pores i-th conductive pores, namely Eq. (43):

$$P_i = \frac{r_{\min i}^2}{r_{mi}^2} \tag{43}$$

In Eq. (43), r_{mi} refers to the average radius value of pores with a pore scaling factor of c_{2i}. Then, define P as the weighted average of P_i of a single truncated cone pore, and define the average pore scaling factor as c_2, which is the weighted average of a single truncated cone pore. After the above definition is given, the following equation is obtained:

$$\sum_{i=1}^{o} f_i c_{2i} r_{\min i}^2 = \sum_{i=1}^{o} f_i P_i c_{2i} r_{mi}^2 = P c_2 \overline{r_m}^2 \tag{44}$$

$\overline{r_m}$ refers to the average values along the radius of the truncated cone pores. Among them, the expression of P is:

$$P = \frac{\overline{r_{\min}}^2}{\overline{r_m}^2} \tag{45}$$

where $\overline{r_{\min}}$ refers to the average values along the radius of the smallest cross section among truncated cone pores.

Substituting Eq. (44) into Eq. (42), Eq. (46) is obtained, which is Eq. (15).

$$
\begin{aligned}
F &= \frac{\tau_e^2}{(1+e)^2}\frac{\overline{r_m}^2}{\varphi_p}\left(Pc_2\overline{r_m}^2\right)^{-1} + \frac{e\tau_e}{(1+e)c_1c_3} \\
&= \frac{\tau_e^2}{(1+e)^2}\frac{\overline{r_m}^2}{\varphi_p}\frac{1}{c_2\overline{r_m}^2P} + \frac{e\tau_e}{(1+e)c_1c_3} \\
&= \frac{\tau_e^2}{(1+e)^2}\frac{\overline{r_m}^2}{Q\varphi}\frac{1}{c_2\overline{r_m}^2P} + \frac{e\tau_e}{(1+e)c_1c_3}
\end{aligned}
\tag{46}
$$

where φ_p is the porosity of the conductive pores. Q can be called an intermediate coefficient, and the equation of Q is as follows:

$$
Q = \frac{\varphi_p}{\varphi} \tag{47}
$$

Appendix 3: Derivation of Eq. (16)

The first step is to solve φ_p. Here, a new parameter e_{ps} is given, which represents the volume ratio of conductive pores to weakly conductive pores. Depending on the settings, there is an equation:

$$
S_1 = e_{ps}c_1c_3eS \tag{48}
$$

According to the assumption, combining Eqs. (5)–(8) and (48), Eq. (49) is obtained:

$$
\begin{cases}
\varphi = \varphi_p + \varphi_h + \varphi_u \\
c_3 = \frac{S_2}{S_2+S_3} = \frac{S_2L_2}{S_2L_2+S_3L_2} \approx \frac{\varphi_h}{\varphi_h+\varphi_u} \\
e_{ps} = \frac{\varphi_p}{\varphi_h}
\end{cases}
\tag{49}
$$

where φ_h refers to the porosity of weakly conductive pores and φ_u refers to the porosity of nonconductive pores. Note that the assumption of $L_2 \approx L_3$ is used here, and Appendix 4 details why we chose to do this. The paper also investigates the effect on the formation factor if $L_2 \approx L_3$ is not recognized and explores whether the actual value of the ratio of L_2 to L_3 is close to 1 based on actual experiment data.

Through these changes, combining Eqs. (6)–(9), by characterizing the volume of pores, the calculation equations of the ratio of 3 pore types are obtained:

$$
\begin{cases}
Q = \frac{\varphi_p}{\varphi} = \frac{c_3e_{ps}}{1+c_3e_{ps}} \\
\frac{\varphi_h}{\varphi} = \frac{c_3}{1+c_3e_{ps}} \\
\frac{\varphi_u}{\varphi} = 1 - \frac{\varphi_p}{\varphi} - \frac{\varphi_h}{\varphi}
\end{cases}
\tag{50}
$$

φ is characterized as follows:

$$
\varphi = \frac{S_1L_1}{SL} + \frac{S_2L_2 + S_3L_3}{SL} = \frac{\tau_e}{1+e}e_{ps}ec_1c_3 + \frac{e\tau_e}{1+e}c_1 \tag{51}
$$

According to Eq. (51):

$$e = \frac{\varphi}{c_1\tau_e + c_1c_3e_{ps}\tau_e - \varphi} \tag{52}$$

Considering the equivalence only from a volume perspective, the conductive pores are equivalent to a cylinder with a circular cross section whose porosity is consistent with the conductive pores. Then, the corresponding equation can be written:

$$\pi P\overline{r_{\min}}^2 L_1 = \frac{1}{3}\pi L_1\left(\overline{r_{\min}}^2 + \overline{r_{\max}}^2 + \overline{r_{\min}r_{\max}}\right) \tag{53}$$

In this way, the information of the truncated cone pores in the formation factor can be guaranteed, and the shape of the conductive pores is mathematically restricted. Since Eq. (53) is obtained only from the concept of volume, without any information about pore conductivity, it is eternal true. The right side of Eq. (53) is the volume formula of the truncated cone. Combining Eq. (38), the equation can be obtained according to Eq. (53):

$$P = \frac{3}{1 + c_2 + c_2^2} \tag{54}$$

Substituting Eqs. (52)–(54) into Eq. (15) yields the following:

$$F = \frac{\left(c_1\tau_e + c_1c_3e_{ps}\tau_e - \varphi\right)^2\left(1 + c_2 + c_2^2\right)}{3c_1^2c_2c_3e_{ps}\left(1 + c_3e_{ps}\right)}\frac{1}{\varphi} + \frac{\varphi}{\left(1 + c_3e_{ps}\right)c_1^2c_3} \tag{55}$$

Equation (55) is also Eq. (16).

Appendix 4: Assume that $L_2 \approx L_3$ in the model

In theory, the weakly conductive and nonconductive pores do not differ much in length from each other, while the pore length of the conductive pores is much greater than them, because of the particularity of their locations and occurrence.

In addition, the coefficient z is increased, which reflects the relationship between L_3 and L_2, $zL_2 = L_3$. The relationship between L_3 and L_2 can be disproved by the value of z. All other assumptions are consistent with those in Eqs. (5), (6) and (48), and a new formation factor expression is obtained on this basis. Since the nonconductive pores do not directly affect the rock conductivity but indirectly affect the formation factor, the following equation, Eq. (56), is obtained:

$$\varphi = \frac{S_1L_1}{SL} + \frac{S_2L_2 + S_3L_3}{SL} = \frac{S_1L_1}{SL} + \frac{S_2L_2 + zS_3L_2}{SL} = \frac{\left(1 + e_{ps}\right)c_1c_3e\tau_e + c_1\left(1 - c_3\right)ez\tau_e}{1 + e} \tag{56}$$

Equation (56) is transformed to obtain Eq. (57):

$$e = \frac{\varphi}{\left(1 + e_{ps}\right)c_1c_3\tau_e + c_1\left(1 - c_3\right)ez\tau_e - \varphi} \tag{57}$$

Then, combine Eq. (57), substitute into Eq. (46), perform a formula transformation, and finally, the formation factor formula is obtained:

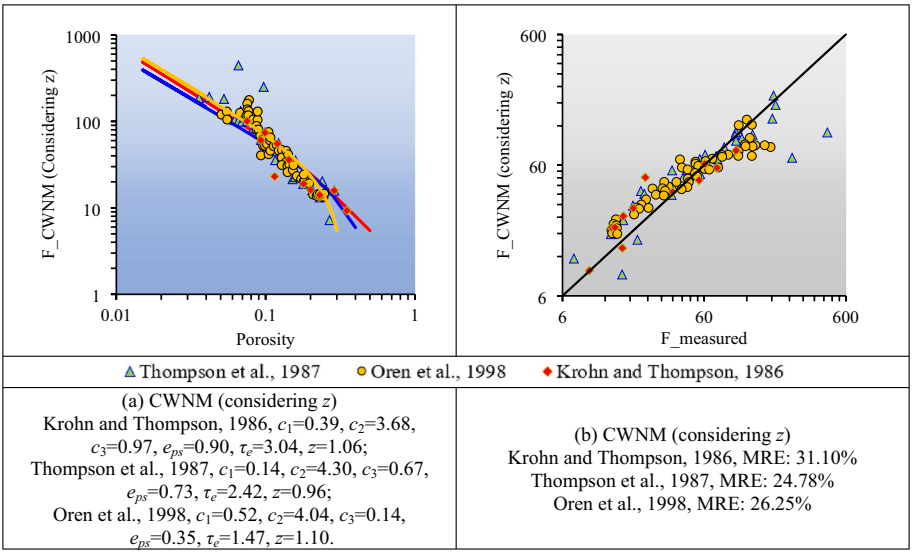

(a) CWNM (considering z)
Krohn and Thompson, 1986, c_1=0.39, c_2=3.68, c_3=0.97, e_{ps}=0.90, τ_e=3.04, z=1.06;
Thompson et al., 1987, c_1=0.14, c_2=4.30, c_3=0.67, e_{ps}=0.73, τ_e=2.42, z=0.96;
Oren et al., 1998, c_1=0.52, c_2=4.04, c_3=0.14, e_{ps}=0.35, τ_e=1.47, z=1.10.

(b) CWNM (considering z)
Krohn and Thompson, 1986, MRE: 31.10%
Thompson et al., 1987, MRE: 24.78%
Oren et al., 1998, MRE: 26.25%

Fig. 11 Solving for the formation factor of the conventional medium- to high-porosity sandstone considering z

$$F = \frac{\left(3 + e_{ps}\left(1 + c_2 + c_2^2\right)\right)\varphi}{c_1 c_3 e_{ps}\left(1 + c_2 + c_2^2\right)\left(z\left(c_3 - 1\right)c_1 - c_3 - c_1 c_3 e_{ps}\right)} - \frac{3\left(\left((z - e_{ps})c_3 - z\right)c_1 - c_3\right)\tau_e^2}{c_1 c_3 e_{ps}\left(1 + c_2 + c_2^2\right)}\frac{1}{\varphi} - \frac{6\tau_e}{c_1 c_3 e_{ps}\left(1 + c_2 + c_2^2\right)} \tag{58}$$

To explore the value of z based on porous rock data, the data in Sect. 5.1 still be used to optimize the model parameters. Figure 11 shows the model parameter calculation results and the corresponding accuracy results.

From the results of the parameter calculation, the z value is basically stable in the range of 0.95–1.1, which is not much different from 1. From the perspective of accuracy, for the same data, although the formation factor formula given by Eq. (57) gives more parameters than the CWNM, it also considers the large difference between L_3 and L_2. However, the optimization effect has not been significantly improved, which shows that more parameters are not optimal, and more parameters increase the difficulty of parameter selection.

To further prove that the z parameter is not important enough to be considered, the influence of the value of the z parameter on the model is simulated. In this process, we refer to the optimization results of the core data and define the range of z as 0.8–3.5 to observe the change in the relationship between the formation factor and porosity. The final result is shown in Fig. 12. According to the results, the influence of z on the formation factor–porosity relationship is definitely much lower than the influence of c_1, c_2, c_3, e_{ps} and τ_e shown in Fig. 3. Therefore, from this point of view, setting z to 1 does not have an large impact on the model. Although the CWNM does not use Eq. (58) to more comprehensively characterize the pore conductivity, it gives a simplification. However, since the nonconductive pores do not participate in the conductivity of the rock, at least in the case of using the optimization algorithm to solve the parameters, it is sufficient to use c_1 to reflect the characteristics of the nonconductive pores.

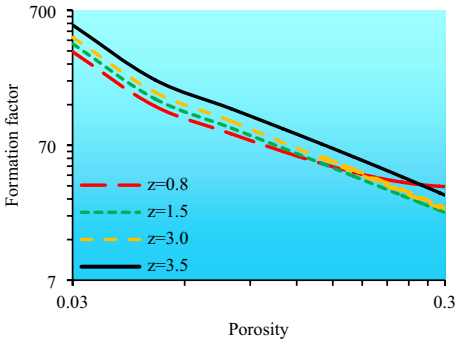

Fig. 12 Changes in z parameter in the CWNM in Appendix 4 and their effect on the formation factor–porosity relationship

(locking c_1=0.3, c_2=4.0, c_3=0.5, e_{ps}=0.6, τ_e=2.5)

Acknowledgements This project was funded by National Natural Science Foundation of China (No. 42106213 and 41722403); China Postdoctoral Science Foundation (Nos. 2021M690161 and 2021T140691); National Key Research and Development Program of China (No. 2021YFC3100601). The authors would like to express their sincere gratitude to the Editor in Chief of Surveys in Geophysics–Prof. Michael J. Rycroft—for his enthusiasm, patience and tireless efforts. The authors are also grateful to the 3 anonymous reviewers for their constructive advice on how to improve the paper. Their earnestness, meticulousness and patience in reviewing this manuscript have been remarkable, and their comments and suggestions have greatly improved all aspects of this article.

Declarations

Conflict of interest The authors declare that they have no known competing financial interests or personal relationships that could have appeared to influence the work reported in this paper.

References

Abderrahmene M, Abdelilah B, Fouad G (2017) Electrical prediction of tortuosity in porous media. Energy Procedia 139:718–724

Adler PM, Jacquin CG, Thovert JF (1992) The formation factor of reconstructed porous media. Water Resour Res 28(6):1571–1576

Al-Mukainah HS, Hussaini SR, Dvorkin JP (2022) Electrical formation factor versus porosity coarse-scale transforms from microscopic digital images: example-based study. J Pet Sci Eng 210:110054

Andrä H, Combaret N, Dvokin J, Glatt E, Han J, Kabel M, Keehm Y, Krzikalla F, Lee M, Madonna C, Marsh M, Mukerji T, Saenger EH, Sain R, Saxena N, Ricker S, Wiegmann A, Zhan X (2013) Digital rock physics benchmarks—part II: computing effective properties. Comput Geosci 50:33–43

Archie GE (1942) The electrical resistivity log as an aid in determining some reservoir characteristics. Trans AIME 146(1):54–62

Attia AM, Fratta D, Bassiouni Z (2008) Irreducible water saturation from capillary pressure and electrical resistivity measurements. Oil Gas Sci Technol 63(2):203–217

Bakar WZW, Saaid IM, Ahmad MR, Amir Z, Mahat SQA (2019) Derivation of formation factor in shaly sandstone with geometry and clay conductivity effects. J Pet Sci Eng 182:106359

Balsamo F, Bezerra FHR, Klimchouk AB, Cazarin CL, Auler AS, Nogueira FC, Pontes C (2020) Influence of fracture stratigraphy on hypogene cave development and fluid flow anisotropy in layered carbonates, NE Brazil. Mar Pet Geol 114:104207

Bauer D, Youssef S, Han M, Bekri S, Rosenberg E, Fleury M, Vizika O (2011) From computed microtomography images to resistivity index calculations of heterogeneous carbonates using a dual-porosity pore-network approach: influence of percolation on the electrical transport properties. Phys Rev E 84(1):011133

Berg CF, Held R (2016) Fundamental transport property relations in porous media incorporating detailed pore structure description. Transp Porous Media 112:467–487

Berg CF, Kennedy WD, Herrick DC (2022) Conductivity in partially saturated porous media described by porosity, electrolyte saturation and saturation-dependent tortuosity and constriction factor. Geophys Prospect 70(2):400-420
Bernabé Y, Li M, Maineult A (2010) Permeability and pore connectivity: a new model based on network simulations. J Geophys Res 115(B10):B10203
Bernabé Y, Li M, Tang Y, Evans B (2016) Pore space connectivity and the transport properties of rocks. Oil Gas Sci Technol 71(4):50
Brown GA (1986) A mathematical comparison of common saturation equations. In: SPWLA 27th annual logging symposium, pp T1–T24
Brown GA (1988) The formation porosity exponent: the key to improved estimates of water saturation in shaly sands. In: SPWLA 29th annual logging symposium, pp AA1–AA10
Bussian AE (1983) Electrical conductance in a porous medium. Geophysics 48(9):1258–1268
Caesary D, Kim J, Jang SJ, Quach N, Park C, Kim H, Nam M (2022) Numerical modeling and evaluation of lab-scale CO_2-injection experiments based on electrical resistivity measurements. J Pet Sci Eng 208:109788
Cai J, Wei W, Hu X, Wood DA (2017) Electrical conductivity models in saturated porous media: a review. Earth-Sci Rev 171:419–433
Cai J, Lin D, Singh H, Wei W, Zhou S (2018) Shale gas transport model in 3D fractal porous media with variable pore sizes. Mar Pet Geol 98:437–447
Cai J, Zhang Z, Wei W, Guo D, Li S, Zhao P (2019) The critical factors for permeability-formation factor relation in reservoir rocks: pore-throat ratio, tortuosity and connectivity. Energy 188:116051
Carman PC (1937) Fluid flow through granular beds. Trans Inst Chem Eng 15:150–167
Chen M, Li M, Bernabé Y, Zhao J, Zhang L, Zhang Z, Zhang Y, Tang Y, Xiao W (2019) Effective pressure law for the intrinsic formation factor in low permeability sandstones. J Geophys Res Solid Earth 122(11):8709–8723
Cheng Y, Zhang C, Zhu L (2017) A fractal irreducible water saturation model for capillary tubes and its application in tight gas reservoir. J Pet Sci Eng 159:731–739
Clavier C, Heim A, Scala C (1976) Effects of pyrite on resistivity and other logging measurements. In: SPWLA 17th annual logging symposium, pp HH1–HH34
Clennell MB, Josh M, Esteban L, Piane CD, Schmid S, Verrall M, Hill D, Woods C, McMullan B (2010) The influence of pyrite on rock electrical properties: a case study from NW Australian gas reservoirs. In: SPWLA 51th annual logging symposium, pp 1–13
Constable S, Lu R, Stern LA, Frane WLD, Roberts JJ (2020) Laboratory electrical conductivity of marine gas hydrate. Geophys Res Lett 47(16):e2020GL087645
Cook AE, Anderson BI, Rasmus J, Sun K, Li Q, Collett TS, Goldberg DS (2012) Electrical anisotropy of gas hydrate-bearing sand reservoirs in the Gulf of Mexico. Mar Pet Geol 34(1):72–84
Cosenza P, Pert D, Zamora M (2015) Effect of the local clay distribution on the effective electrical conductivity of clay rocks. J Geophys Res Solid Earth 120(1):145–168
Daigle H, Ghanbarian B, Henry P, Marianne C (2015) Universal scaling of the formation factor in clays: example from the Nankai Trough. J Geophys Res Solid Earth 120(11):7361–7375
Dong H, Sun J, Zhu J, Liu L, Lin Z, Gelsanami N, Cui L, Yan W (2019) Developing a new hydrate saturation calculation model for hydrate-bearing sediments. Fuel 248:27–37
Dong H, Sun J, Arif M, Golsanami N, Yan W, Zhang Y (2020) A novel hybrid method for gas hydrate filling modes identification via digital rock. Mar Pet Geol 115:104255
Ellis MH, Sinha MC, Minshull TA, Sothcott J, Best AI (2010) An anisotropic model for the electrical resistivity of two-phase geologic materials. Geophysics 75(6):E161–E170
Esmaeilpour M, Ghanbarian B, Liang F, Liu H (2021) Scale-dependent permeability and formation factor in porous media: applications of percolation theory. Fuel 301:121090
Fan Y, Pan B, Zhang F (2018) Research on conductive mechanism and saturation model of the volcanic reservoir with complex pore structure. Geophys Geochem Explor 42(1):172–177
Feng G, Lan Y, Shi Y, Li Y (2022) Numerical simulation for conductivity of low-permeability sandstone based on digital core. Wel Logging Technol 46(4):390–396
Fheed A, Krzyżak A (2017) A textural and diagenetic assessment of the Zechstein Limestone carbonates, Poland using the transverse Nuclear Magnetic Resonance relaxometry. J Pet Sci Eng 152:538–548
Foroozesh J, Abdalla AIM, Zhang Z (2019) Pore network modelling of shale gas reservoirs: gas desorption and slip flow effects. Transp Porous Media 126(3):633–653
Fu C, Wang A (2022) Improvement of new three-water model and determination of its parameter. J Jilin Univ (Earth Science Edition) 52(2):654–661
Fu J, Thomas HR, Li C (2021) Tortuosity of porous media: image analysis and physical simulation. Earth-Sci Rev 212:103439

Gao Z, Fan Y, Xuan Q, Zheng G (2020) A review of shale pore structure evolution characteristics with increasing thermal maturities. Adv Geo-Energy Res 4(3):247–259
Ghanbarian B, Berg CF (2017) Formation factor in Bentheimer and Fontainebleau sandstones: theory compared with pore-scale numerical simulations. Adv Water Resour 107:139–146
Ghanbarian B, Male F (2021) Theoretical power-law relationship between permeability and formation factor. J Pet Sci Eng 198:108249
Ghanbarian B, Hunt AG, Sahimi M, Ewing RP, Skinner TE (2013) Percolation theory generates a physically based description of tortuosity in saturated and unsaturated porous media. Soil Sci Soc Am J 77(6):1920–1929
Ghanbarian B, Hunt AG, Ewing RP, Skinner TE (2014) Universal scaling of the formation factor in porous media derived by combining percolation and effective medium theories. Geophys Res Lett 41(11):3884–3890
Ghanbarian B, Hunt AG, Skaggs TH, Jarvis N (2017) Upscaling soil saturated hydraulic conductivity from pore throat characteristics. Adv Water Resour 104:105–113
Givens WW (1987) A conductive rock matrix model (CRMM) for the analysis of low-contrast resistivity formation. Log Anal 28(2):138–151
Glover PWJ (2010) A generalized Archie's law for n phases. Geophysics 75(6):E247–E265
Glover PWJ (2016) Archie's law-a reappraisal. Solid Earth 7(4):1157–1169
Glover PWJ, Meredith PG, Sammonds PR, Murrell SAF (1994) Lonic surface electrical conductivity in sandstone. J Geophys Res 99(B11):21635–21650
Glover PWJ, Hole MJ, Pous J (2020) A modified Archie's law for two conducting phases. Earth Planet Sci Lett 180(3–4):369–383
Greve AK, Roshan H, Kelly BFJ, Acworth RI (2013) Electrical conductivity of partially saturated porous media containing clay: an improved formulation. J Geophys Res Solid Earth 118(7):3297–3303
Gueguen Y, Dienes J (1989) Transport properties of rock from statistics and percolation. Math Geol 21(1):1–13
Guéguen Y, Palciauskas V (1994) Introduction to the physics of rocks. Princeton University Press, New Jersey
Guo X (2011) Well logging response characteristics and evaluation on gas hydrate in Qilian Mountain Permafrost. Master's thesis of Chinese Academy of Geological Sciences
Guo C, Fan Z, Ling B, Yang Z (2021) A tensorial Archie's law for water saturation evaluation in anisotropic model. IEEE Geosci Remote Sens Lett 19:8024505
Guo Y, Pan B, Zhang L, Lei J, Fan Y, Ruhan A, Yan D, Zhao Y (2022) A study on water saturation predictions in igneous reservoirs based on the relationship between the transverse relaxation time and the resistivity index. J Pet Sci Eng 208:109519
Hakimov N, Zolfaghari A, Kalantari-Dahaghi A, Negahban S, Gunter G (2019) Pore-scale network modeling of microporosity in low-resistivity pay zones of carbonate reservoir. J Nat Gas Sci Eng 71:103005
Han T, Clennell MB, Pervukhina M (2015) Modelling the low-frequency electrical properties of pyrite-bearing reservoir sandstones. Mar Pet Geol 68:341–351
He S, Zhang H, Yang D, Wu Y, Wu J (2017) Experiment and application of rock electrical experiment with different gas components under high temperature and high pressure condition. Nat Gas Geosci 28(4):575–581
He R, Ma H, Hafiz RB, Fu C, Jin X, He J (2018) Determining porosity and pore network connectivity of cement-based materials by a modified non-contact electrical resistivity measurement: experiment and theory. Mater Des 156:82–92
Herrick DC, Kennedy WD (2009) A new look at electrical conduction in porous media: a physical description of rock conductivity. In: SPWLA 50th annual logging symposium, pp 1–15
Hematpur H, Abdollahi R, Rostami S, Haghighi M, Blunt M (2023) Review of underground hydrogen storage: concepts and challenges. Adv Geo-Energy Res 7(2):111–131
Holland J (1975) Adaptation in natural and artificial systems: an introductory analysis with application to biology. The University of Michigan Press, Michigan
Hu S, Zhou C, Li X, Li C, Zhang S (2017) A tight sandstone trapezoidal pore oil saturation model. Pet Explor Dev 44(5):876–886
Hu X, Zou C, Lu Z, Yu C, Peng C, Li W, Tang Y, Liu A, Kouamelan KS (2019) Evaluation of gas hydrate saturation by effective medium theory in shaly sands: a case study from the Qilian Mountain permafrost, China. J Geophys Eng 16(1):215–228
Hunt AG (2004) Continuum percolation theory and Archie's law. Geophys Res Lett 31(19):L19503
Iheanacho PC (2014) Formation-resistivity theory: how Archie equations, shaly-reservoir models, conductive rock-matrix model, and dual-triple-porosity models are related. SPE Reserv Eval Eng 17(2):141–151

Jackson PD, Briggs KB, Flint RC, Holyer RJ, Sandidge JC (2002) Two- and three-dimensional heterogeneity in carbonate sediments using resistivity imaging. Mar Geol 182(1–2):55–76
Jiao L, Andersen PØ, Zhou J, Cai J (2020) Applications of mercury intrusion capillary pressure for pore structures: a review. Capillarity 3(4):62–74
Jin Y, Li S, Yang D (2020) Experimental and theoretical quantification of the relationship between electrical resistivity and hydrate saturation in porous media. Fuel 269:117378
Kennedy W, Herrick D (2012) Conductivity models for Archie rocks. Geophysics 77(3):WA109–WA128
Kirkpatrick S (1973) Percolation and conduction. Rev Mod Phys 45(4):574–588
Kolah-kaj P, Kord S, Soleymanzadeh A (2021) The effect of pressure on electrical rock typing, formation resistivity factor, and cementation factor. J Pet Sci Eng 204:108757
Krohn CE, Thompson AH (1986) Fractal sandstone pores: automated measurements using scanning-electron-microscope images. Phys Rev B Condens Matter 33(9):6366–6374
Lai J, Pang X, Xu F, Wang G, Fan X, Xie W, Chen J, Qin Z, Zhou L (2019) Origin and formation mechanisms of low oil saturation reservoirs in Nanpu Sag, Bohai Bay Basin, China. Mar Pet Geol 110:317–334
Lala AMS (2020) A novel model for reservoir rock tortuosity estimation. J Pet Sci Eng 192:107321
Lee H, Lee J, Oh T (2021) Permeability evaluation for artificial single rock fracture according to geometric aperture variation using electrical resistivity. J Rock Mech Geotech Eng 13(4):787–797
Li N (1989) General forms of the resistivity-porosity and resistivity-oil/gas saturation relations, as well as the determination of their optimum approximating function types (I). Chin J Geophys 65(4):1482–1493
Li S, Hou S (2019) A brief review of the correlation between electrical properties and wetting behaviour in porous media. Capillarity 2(3):53–56
Li X, Zhao W, Zhou C, Wang T, Li C (2012) Dual-porosity saturation model of low-porosity and low-permeability clastic reservoirs. Pet Explor Dev 39(1):88–98
Li X, Qin R, Mao Z, Liu C (2014) Establishment and application of a high-precision cementation exponent model. Acta Petrol Sin 35(1):76–84
Li W, Zou C, Wang H, Peng C (2017) A model for calculating the formation resistivity factor in low and middle porosity sandstone formations considering the effect of pore geometry. J Pet Sci Eng 152:193–203
Li K, Hou B, Bian H, Liu H, Wang C, Xie R (2019) Verification of model for calculating capillary pressure from resistivity using experimental data. Fuel 252:281–294
Li X, Li C, Li B, Liu X, Yuan C (2020) Response laws of rock electrical property and saturation evaluation method of tight sandstone. Pet Explor Dev 47(1):214–224
Li B, Nie X, Cai J, Zhou X, Wang C, Han D (2022) U-Net model for multi-component digital rock modeling of shales based on CT and QEMSCAN images. J Pet Sci Eng 216:110734
Liu T, Tang T, Du H, Zhang H, Wang H (2013) Study of rock conductive mechanism based on pore structure. Chin J Geophys 56(5):674–684
Liu X, Wang J, Ge L, Hu F, Li C, Li X, Yi J, Xu H, Li S, Xue Q (2017) Pore-scale characterization of tight sandstone in Yanchang Formation Ordos Basin China using micro-CT and SEM imaging from nm- to cm-scale. Fuel 209:254–264
Liu Z, Zhang C, Tang J, Xiao C (2018) Influence of fracture on rock resistivity and its application in saturation calculation. Litho Reserv 201:108530
Liu L, Zhang Z, Li C, Ning F, Liu C, Wu N, Cai J (2020) Hydrate growth in quartzitic sands and implication of pore fractal characteristics to hydraulic, mechanical, and electrical properties of hydrate-bearing sediments. J Nat Gas Sci Eng 75:103109
Liu X, Yan J, Zhang X, Zhang L, Ni H, Zhou W, Wei B, Li C, Fu L (2021) Numerical upscaling of multi-mineral digital rocks: electrical conductivities of tight sandstones. J Pet Sci Eng 201:108530
Mahmoodpour S, Kamari E, Esfahani MR, Mehr AK (2021) Prediction of cementation factor for low-permeability Iranian carbonate reservoirs using particle swarm optimization-artificial neural network model and genetic programming algorithm. J Pet Sci Eng 197:108102
Malekimostaghim E, Gholami R, Rezaee R, Asef MR, Zhong ZQ, Sarmadivaleh M (2019) A laboratory-based approach to determine Archie's cementation factor for shale reservoirs. J Pet Sci Eng 183:106399
Mawer C, Knight R, Kitaniais PK (2015) Relating relative hydraulic and electrical conductivity in the unsaturated zone. Water Resour Res 51(1):599–618
Meng H (2018) Study on the rock-electric and the relative permeability characteristics in porous rocks based on the curved cylinder-sphere model. J Pet Sci Eng 166:891–899
Meng H, Liu T (2019) Interpretation of the rock-electric and seepage characteristics using the pore network model. J Pet Sci Eng 180:1–10

Mo X, He D, Li Z, Wen X, Li G (2001) The application of three-water conduction model in the interpretation of low-resistivity reservoir. J Changchun Univ Sci Eng 31(1):92–95
Müller-Huber E, Schön J, Börner F (2015) The effect of a variable pore radius on formation resistivity factor. J Appl Geophys 116:173–179
Mustofa MB, Fauzi U, Latief FDE, Warse W (2022) Experimental and modeling of electrical resistivity changes due to micro-spatial distribution of fluid for unconsolidated sand. J Pet Sci Eng 208:109472
Nazemi M, Tavakoli V, Sharifi-Yazdi M, Rahimpour-Bonab H, Hosseini M (2019) The impact of micro-to macro-scale geological attributes on Archie's exponents, an example from Permian-Triassic carbonate reservoirs of the central Persian Gulf. Mar Pet Geol 102:775–785
Nie X, Zou C, Li Z, Meng X, Qi X (2016) Numerical simulation of the electrical properties of shale gas reservoir rock based on digital core. J Geophys Eng 13:481–490
Nishiyama N, Yokoyama Y (2017) Permeability of porous media: role of the critical pore size. J Geophys Res Solid Earth 122(9):6955–6971
Olsen C, Hongdul T, Fabricius L (2008) Prediction of Archie's cementation factor from porosity and permeability through specific surface. Geophysics 73(2):E81–E87
Øren PE, Bakke S, Arntzen OJ (1998) Extending predictive capabilities to network models. SPE J 3(4):324–336
Pan B, Liu S, Huang B, Fang C, Guo Y (2016) Application of the CEC ratio method in evaluation of tuffaceous sandstone reservoirs: an example in the X depression of Hailar-Tamtsag basin. Chin J Geophys 59(4):373–381
Pang M, Ba J, Carcione J, Balcewicz M, Yue W, Saenger EH (2022) Acoustic and electrical properties of tight rocks: a comparative study between experiment and theory. Surv Geophys 43:1761–1791
Paterson MS (1983) The equivalent channel model for permeability and resistivity in fluid-saturated rock—a re-appraisal. Mech Mater 2(4):345–352
Patnode HW, Wylie MRJ (1950) The presence of conductive solids in reservoir rocks. J Pet Technol 2(2):47–52
Pei F, He D, Fang H, Wang X, Qiu G, Zhang X, He M, Zhang Y, Wang G (2022) Comparative study of the electrical characteristics of hydrate reservoirs before and after gas hydrate trial production in the Muli permafrost area of the Qilian Mountains, NW China. Cold Reg Sci Technol 198:103551
Permyakov ME, Manchenko NA, Duchkov AD, Manakov AY, Drobchik AN, Manshtein AK (2017) Laboratory modeling and measurement of the electrical resistivity of hydrate-bearing sand samples. Russ Geol Geophys 58(5):642–649
Piedrahita J, Aguilera R (2017) A petrophysical dual-porosity model for evaluation of secondary mineralization and tortuosity in naturally fractured reservoirs. SPE Reserv Eval Eng 20(2):304–316
Qiao J, Zeng J, Chen D, Cai J, Jiang S, Xiao E, Zhang Y, Feng X, Feng S (2022) Permeability estimation of tight sandstone from pore structure characterization. Mar Pet Geol 135:105382
Qin Z, Pan H, Ma H, Konaté AA, Hou M, Luo S (2016) Fast prediction method of Archie's cementation exponent. J Nat Gas Sci Eng 34:291–297
Rahman T, Lebedev M, Zhang Y, Barifcani A, Iglauer S (2017) Influence of rock microstructure on its electrical properties: an analysis using x-ray microcomputed tomography. Energy Procedia 114:5023–5031
Regnet JB, Robion P, David C, Fortin J, Brigaud B, Yven B (2015) Acoustic and reservoir properties of microporous carbonate rocks: implication of micrite particle size and morphology. J Geophys Res Solid Earth 120:790–811
Rembert F, Jougnot D, Guarracino L (2020) A fractal model for the electrical conductivity of water-saturated porous media during mineral precipitation–dissolution processes. Adv Water Resour 145:103742
Revil A, Glover PWJ (1998) Nature of surface electrical conductivity in natural sands sandstones, and clays. Geophys Res Lett 25(5):691–694
Revil A, Cathles LM, Losh S, Nunn JA (1998) Electrical conductivity in shaly sands with geophysical applications. J Geophys Res 103(B10):23925–23936
Revil A, Kessouri P, Torres-Verdín C (2014) Electrical conductivity, induced polarization, and permeability of the Fontainebleau sandstone. Geophysics 79(5):D301–D318
Revil A, Ahmed AS, Matthai S (2018) Transport of water and ions in partially water-saturated porous media. Part 3. Electrical conductivity. Adv Water Resour 121:97–111
Riedel M, Collett TS, Kim HS, Bahk JJ, Kim JH, Ryu BJ, Kim GY (2013) Large-scale depositional characteristics of the Ulleung Basin and its impact on electrical resistivity and Archie-parameters for gas hydrate saturation estimates. Mar Pet Geol 47:222–235

Rocha HO, Costa JLS, Carrasquilla AAG (2019) Petrophysical characterization using well log resistivity and rock grain specific surface area in a fractured carbonate pre-salt reservoir in the Santos Basin, Brazil. J Pet Sci Eng 183:106372

Roozshenas AA, Miri R, Kord S (2022) Improved prediction of hydrologic properties of heterogeneous porous media at pore-scale—a multi-physics lattice Boltzmann study. Sustain Energy Technol Assess 52:102101

Ruffet C, Darot M, Gueguen Y (1995) Surface conductivity in rocks: a review. Surv Geophys 16(1):83–105

Sawayama K, Ishibashi T, Jiang F, Tsuji Y, Nishizawa O, Fujimitsu Y (2021a) Scale-independent relationship between permeability and resistivity in mated fractures with natural rough surfaces. Geothermics 94:102065

Sawayama K, Ishibashi T, Jiang F, Tsuji Y, Fujimitsu Y (2021b) Relating hydraulic–electrical–elastic properties of natural rock fractures at elevated stress and associated transient changes of fracture flow. Rock Mech Roch Eng 54:2145–2164

Saxena N, Dietderich J, Alpak FO, Hows A, Appel M, Freeman J, Hofmann R, Zhao B (2021) Estimating electrical cementation and saturation exponents using digital rock physics. J Pet Sci Eng 198:108198

Sen P, Scala C, Cohen MH (1981) A self-similar model for sedimentary rocks with application to the dielectric constant of fused glass beads. Geophysics 46:781–795

Sevostianov I, Trofimov A, Merodio J, Penta R, Rodriguez-Ramos R (2017) Connection between electrical conductivity and diffusion coefficient of a conductive porous material filled with electrolyte. Int J Eng Sci 121:108–117

Shahsenov IS, Orujov GI (2018) Modeling of the cementation factor and hydraulic permeability using Mercury Injection Capillary Pressure (MICP) measurements. J Pet Sci Eng 171:1033–1040

Shang B, Hamman J, Caldwell D (2003) A physical model to explain the first Archie relationship and beyond. In: SPE annual technical conference and exhibition, pp MS1–MS11

Siddiqui MAQ, Ueda K, Komatsu H, Shimamoto T (2020) Caveats of using fractal analysis for clay rich pore spaces. J Pet Sci Eng 195:107622

Silva MTQSD, Caardoso MDR, Veronese CMP, Mazer W (2022) Tortuosity: a brief review. Mater Today Proc 58(4):1344–1349

Soleymanzadeh A, Jamialahmadi M, Helalizadeh A, Soulgani BS (2018) A new technique for electrical rock typing and estimation of cementation factor in carbonate rocks. J Pet Sci Eng 166:381–388

Song Y, Kausik R (2019) NMR application in unconventional shale reservoirs—a new porous media research frontier. Prog Nucl Magn Reson Spectrosc 112–113:17–33

Song Y, Zhang X, Song Y, Zhang Y (2014) On effective medium conductivity model based on non-efficient electrical pore for tight sandy conglomerate reservoirs. Prog Geophys 29(1):209–216

Stenzel O, Pecho O, Holzer L, Neumann M, Schmidt V (2016) Predicting effective conductivities based on geometric microstructure characteristics. AIChE J 62:1834–1843

Stern L, Constable S, Lu R, Frane WLD, Roberts JJ (2021) Electrical properties of carbon dioxide hydrate: implications for monitoring CO_2 in the gas hydrate stability zone. Geophys Res Lett 48(15):e2021GL093475

Sun W, Wong T (2018) Prediction of permeability and formation factor of sandstone with hybrid lattice Boltzmann/finite element simulation on microtomographic images. Int J Rock Mech Min Sci 106:269–277

Sun Z, Mehmani A, Torres-Verdin C (2021) Pore-scale investigation of the electrical resistivity of saturated porous media: flow patterns and porosity efficiency. J Geophys Res Solid Earth 126(12):e2021JB022608

Tang Y, Li M, Bernabé Y, Tang H, Li X, Bai X, Tao Z (2015) A new electrical formation factor model for bimodal carbonates: numerical studies using dual-pore percolation network. Geophys J Int 201(3):1456–1470

Tang T, Lu T, Zhang H, Jiang L, Liu T, Meng H, Wang F (2017a) Electrical characteristics of rocks in fractured and caved reservoirs. J Geophys Eng 14(6):1437–1444

Tang Y, Li M, Li X (2017b) Connectivity, formation factor and permeability of 2D fracture network. Physica A 483(1):319–329

Tariq Z, Mohmoud M, Al-Youssef H, Khan MR (2020) Carbonate rocks resistivity determination using dual and triple porosity conductivity models. Petroleum 6(1):35–42

Thanh L, Jougnot D, Do P, Nghia NVA (2019) A physically based model for the electrical conductivity of water-saturated porous media. Geophys J Int 219:866–876

Thompson AH, Katz AJ, Krohn CE (1987) The microgeometry and transport properties of sedimentary rock. Adv Phys 36(5):625–694

Tian H, Wang G, Wang K, Feng Q, Wu H, Feng Z (2020) Study on the effect of pore structure on resistivity of carbonate reservoirs. Chin J Geophys 63(11):4232–4243

Vialle S, Contraires S, Zinzsner B, Clavaud JB, Mahiouz K, Zuddas P, Zamora M (2014) Percolation of CO_2-rich fluids in a limestone sample: evolution of hydraulic, electrical, chemical, and structural properties. J Geophys Res Solid Earth 119(4):2828–2847

Walsh JB, Brace WF (1984) The effect of pressure on porosity and the transport properties of rock. J Geophys Res Solid Earth 89(B11):9425–9431

Wang H (2018) An improved dual-porosity model for the electrical analysis of fractured porous media based on the pore scale method. J Appl Geophys 159:497–505

Wang H, Zhang J (2019) The effect of various lengths of pores and throats on the formation resistivity factor. J Appl Geophys 162:35–46

Wang Y, Kou X, Feng J, Li X, Zhang Y (2020) Sediment deformation and strain evaluation during methane hydrate dissociation in a novel experimental apparatus. Appl Energy 262:114397

Watanabe K, Flury M (2008) Capillary bundle model of hydraulic conductivity for frozen soil. Water Resour Res 44(12):W12402

Waxman MH, Smits LJM (1968) Electrical conductivities in oil-bearing shaly sands. SPE J 8(2):107–122

Wei W, Cai J, Hu X, Han Q (2015) An electrical conductivity model for fractal porous media. Geophys Res Lett 42(12):4833–4840

Winsauer WO, Shearin JrHM, Masson PY, Williams M (1952) Resistivity of brine-saturated sands in relation to pore geometry. AAPG Bull 36(2):253–277

Wu Y, Lin C, Yan W, Liu Q, Zhao P, Ren L (2020) Pore-scale simulations of electrical and elastic properties of shale samples based on multicomponent and multiscale digital rocks. Mar Pet Geol 117:104369

Wu Y, Tahmasebi P, Lin C, Dong C (2022) Using digital rock physics to investigate the impacts of diagenesis events and pathways on rock properties. J Pet Sci Eng 208:108025

Xiao Z, Yang D, Yuan Y, Yang B, Liu X (2008) Fractal pore network simulation on the drying of porous media. Dry Technol 26(6):651–665

Xie W, Yin Q, Pang X, Wang G, Wang S (2022) The effects of pore structure on the electrical properties of sand-based porous media. Arab J Geosci 15:36

Xu W, Jiao Y (2019) Theoretical framework for percolation threshold, tortuosity and transport properties of porous materials containing 3D non-spherical pores. Int J Eng Sci 134:31–46

Yang R, Hao F, He S, He C, Guo X, Yi J, Hu H, Zhang S, Hu Q (2017) Experimental investigations on the geometry and connectivity of pore space in organic-rich Wufeng and Longmaxi shales. Mar Pet Geol 84:225–242

Yang L, Ai L, Xue K, Ling Z, Li Y (2018) Analyzing the effects of inhomogeneity on the permeability of porous media containing methane hydrates through pore network models combined with CT observation. Energy 163:27–37

Yang X, Du Y, Xu Q, Wu F, Zhou T, Zhao C (2022) Pores integrated fractal (PIF) analysis on transportation in porous media considering spatial distribution of pores and genuine tortuosity. Int J Heat Mass Transf 187:122528

Yue W, Tao G (2013) A new non-Archie model for pore structure: numerical experiments using digital rock models. Geophys J Int 195(1):282–291

Zambrano M, Volatlli T, Mancini L, Pitts A, Giorgioni M, Tondi E (2021) Pore-scale dual-porosity and dual-permeability modeling in an exposed multi-facies porous carbonate reservoir. Mar Pet Geol 128:105004

Zhang Z (2020) Theoretical roots of Archie equations. Prog Geophys 35(4):1514–1522

Zhang Z, Weller A (2014) Fractal dimension of pore-space geometry of an Eocene sandstone formation. Geophysics 79(6):D377–D387

Zhang C, Zhang Z, Li J, Yan W, Li H, Qin H, Lu H, Gu B, Chen H (2010a) Study on electrical conduction mechanism and water saturation equation based on gulf effect. J Oil Gas Technol 31(6):86–90

Zhang L, Pan B, Li Z, Mo X, Xia Z, Xu W (2010b) New three-water conduction model and its application in evaluation of low porosity and low permeability reservoir. Oil Geohys Prospect 45(3):431–435

Zhang C, Guo C, Song Q, Chen Y, Zhu L (2016a) A novel method to predict formation factor using mercury injection data. J China Univ Min Technol 45(4):747–753

Zhang C, Zhang C, Zhang Z, Wu Y, Chen Y, Xing Y, Li C (2016b) Calculation method of water saturation of low-permeability glutenite reservoir and its application: taking the reservoir of Denglouku Formation in Xiaochengzi Area, Wangfu Fault. J Xi'an Shiyou Univ (Natural Science) 31(2):11–17

Zhang B, Wen H, Qing H, Yang K, Luo Y, Yang H, Wang P, He L, Xiao W (2022) The influence of depositional and diagenetic processes on rock electrical properties: a case study of the Longmaxi shale in the Sichuan Basin. J Pet Sci Eng 211:110119

Zhong Z, Rezaee R, Esteban L, Josh M, Feng R (2021) Determination of Archie's cementation exponent for shale reservoirs; an experimental approach. J Pet Sci Eng 201:108527
Zhong Z, Rezaee R, Josh M, Esteban L, Sarmadivaleh M (2022) The salinity dependence of electrical conductivity and Archie's cementation exponent in shale formations. J Pet Sci Eng 208:109324
Zhou J, He S, Chen Y, Cai M, Du X (2017) A study on acoustic velocity and resistivity of rocks in CO_2/natural gas accumulation. J Southwest Pet Univ (Science & Technology Edition) 39(1):73–79
Zhou X, Zhang C, Zhang Z, Zhang R, Zhu L, Zhang C (2019) A saturation evaluation method in tight gas sandstones based on diagenetic facies. Mar Pet Geol 107:310–325
Zhou X, Zhang Z, Zhang C (2022) Comparative study and discussion of diagenetic facies and conductivity characteristics based on experiments. R Soc Open Sci 9(2):202122
Zhu L, Zhang C, Zhang C, Zhou X, Zhang Z, Nie X, Liu W, Zhu B (2019) Challenges and prospects of digital core-reconstruction research. Geofluids 2019:7814180
Zhu L, Ma Y, Cai J, Zhang C, Wu S, Zhou X (2021) Key factors of marine shale conductivity in southern China—Part I: the influence factors other than porosity. J Pet Sci Eng 205:108698
Zhu L, Ma Y, Cai J, Zhang C, Wu S, Zhou X (2022) Key factors of marine shale conductivity in southern China—Part II: the influence of pore space and the development direction of shale gas saturation models. J Pet Sci Eng 209:109516

Authors and Affiliations

Linqi Zhu[1,2] · Shiguo Wu[1,2] · Chaomo Zhang[3] · Siddharth Misra[4,5] · Xueqing Zhou[1,2] · Jianchao Cai[6]

1 Laboratory of Marine Geophysics and Georesources of Hainan Province, Institute of Deep-Sea Science and Engineering, Chinese Academy of Sciences, 572000 Sanya, China

2 Southern Marine Science and Engineering Guangdong Laboratory (Zhuhai), 519000 Zhuhai, China

3 Key Laboratory of Exploration Technologies for Oil and Gas Resources, Ministry of Education, Yangtze University, 430100 Wuhan, China

4 Harold Vance Department of Petroleum Engineering, Texas A&M University, College Station, TX 77843, USA

5 Department of Geology and Geophysics, Texas A&M University, College Station, TX 77843, USA

6 State Key Laboratory of Petroleum Resources and Prospecting, China University of Petroleum, 102249 Beijing, China